buildings

MDPI

Article

Synergistic Optimization of Daylighting and Thermal Performance and Heterogeneous Design Strategies for Teaching Buildings with Different Exterior-Corridor Orientations

Shuyuan Mai [1,*], Xiongjun Tao [1] and Ming Yang [2]

[1] School of Architecture and Art, Guangxi Arts University, Nanning 530007, China; 18378847770@163.com
[2] School of Architecture, Yantai University, Yantai 264000, China; 18363235968@s.ytu.edu.cn
* Correspondence: shuyuan_mai@163.com

Abstract

Reducing operational energy use in teaching buildings is an important way to lower carbon emissions from buildings. For teaching buildings with exterior corridors in Guangzhou, corridor orientation changes solar exposure, shading, and daylight conditions, making it difficult to improve daylighting and cooling performance using the same design strategy. This study examines typical linear teaching buildings with exterior corridors in Guangzhou through parametric modeling, building performance simulation, multi-objective optimization, and machine-learning classification. Compared with the baseline, the overall optimal north-facing-corridor solution increased spatial daylight autonomy and useful daylight illuminance by 0.104 and 0.097, respectively, and reduced cooling energy consumption intensity by 12.35%. The corresponding south-facing-corridor solution increased the two daylighting measures by 0.068 and 0.018 and reduced cooling energy consumption intensity by 19.40%. The high-performance solutions occupied different parameter ranges: classroom depth was mainly 8.5–9.0 m and corridor width 2.6–2.8 m for the south-facing corridor, where the wider corridor provided self-shading; for the north-facing corridor, classroom depth was 8.5–10.0 m and corridor width mainly 2.2–2.6 m. The multilayer perceptron classifier achieved a harmonic mean of precision and recall of approximately 0.98, supporting rapid screening during early-stage design. Feature-attribution analysis showed that classroom depth made the largest contribution to high-performance classification for the north-facing corridor, whereas corridor-side window-to-wall ratio contributed most for the south-facing corridor. Thus, corridor orientation was associated with differences in performance values, favorable parameter distributions, and design-parameter priorities. Within the sampled design space of the Guangzhou case, the same parameter-adjustment sequence should not be applied to both corridor configurations.

Keywords: teaching buildings; daylighting and thermal performance; heterogeneity; multi-objective optimization; classification-based prediction model

Check for updates

Academic Editor: Haifeng Liao

Received: 23 September 2026
Revised: 16 October 2026
Accepted: 20 October 2026
Published: 24 October 2026

Copyright: © 2026 by the authors. Licensee MDPI, Basel, Switzerland. This article is an open access article distributed under the terms and conditions of the Creative Commons Attribution (CC BY) license.

1. Introduction

1.1. Background and Related Work

Buildings and construction remain major sources of global energy consumption and carbon emissions. According to the latest report by the United Nations Environment Programme and the Global Alliance for Buildings and Construction, the sector accounts for approximately 37% of global carbon dioxide emissions; operational carbon emissions from

buildings rose by approximately 1% in 2024 to 9.9 GtCO2. Despite continued improvements in building energy efficiency, progress remains insufficient to meet the pathway to net zero emissions by 2050. Reducing operational energy use and carbon emissions therefore remains an important task in the low-carbon transition of the building sector [1].

Among campus building types, teaching buildings have become the most common spatial prototype in this region because of their potential for natural ventilation, efficient spatial organization, and adaptability [2]. In actual operation, the exterior corridor is not simply a circulation space connecting classrooms. It also acts as a transitional interface that regulates direct solar radiation and the local building microclimate [3,4]. More broadly, recent campus-scale studies have shown that the microclimatic conditions of outdoor spaces between educational buildings can affect thermal comfort and building energy performance, highlighting the close relationship between local microclimate regulation and energy demand [5]. Different exterior corridor orientations, such as north-facing and south-facing corridors, can lead to clear spatial heterogeneity in the amount of solar radiation received by the building envelope and in local air temperature. For example, when the corridor is arranged on a specific side of the building, its overhang depth forms a substantial physical shading element. The resulting changes in local microclimate and radiation conditions create a complex design challenge for teaching buildings: maintaining daylight quality, as measured by spatial daylight autonomy (sDA) and useful daylight illuminance (UDI), while controlling cooling energy consumption intensity (Ec) [6–8]. Therefore, the coupled daylighting and thermal performance of teaching buildings under different exterior corridor orientations requires further investigation.

Existing studies on building performance optimization (BPO) have extensively investigated the effects of passive design parameters on building energy consumption and daylighting performance [9]. Regarding daylighting assessment, several studies have focused on the effects of window-to-wall ratio and shading devices on natural daylighting in educational buildings. For example, Sedaghatnia et al. [10] systematically simulated and investigated the effects of different shading-device dimensions on indoor daylight availability in educational buildings. Mangkuto et al. [11] conducted parametric optimization of window-to-wall ratio, orientation, and wall reflectance for buildings in tropical climates to determine favorable design combinations for improving Useful Daylight Illuminance (UDI). Ochoa et al. [12] further investigated multi-criteria optimization strategies for window design that provide high visual comfort while maintaining low lighting energy consumption, and showed that the trade-off in window proportion was constrained by a distinct threshold. However, most existing daylighting studies have focused on conventional homogeneous office spaces or standard teaching spaces [13,14], while research specifically addressing teaching buildings with exterior corridors remains limited in scope. Most studies are confined to static analyses of local daylight conditions [15] and have not systematically characterized the spatial distribution patterns and heterogeneous differences in daylighting performance induced by linear exterior corridors under different orientations.

Regarding the thermal environment, previous studies have extensively investigated the effects of climate-responsive passive design on building cooling energy consumption. For example, Zomorodian et al. [16] comprehensively reviewed thermal comfort assessment in educational buildings and emphasized the importance of climate-responsive design in reducing school energy consumption. Hwang et al. [17] conducted long-term field measurements in campus classrooms located in a subtropical climate similar to that of Guangzhou and quantified the potential of passive climate-adaptive strategies to improve the indoor thermal environment. Tzempelikos and Athienitis [18] further investigated the coupled effects of façade shading design and control strategies in balancing cooling-load and lighting-energy demands. However, for teaching buildings with exterior corridors in

hot-summer and warm-winter regions such as Guangzhou, existing thermal-environment studies have largely focused on macro-scale calculations of whole-building energy consumption, with limited attention paid to differences in how the thermal environment evolves under different exterior-corridor orientations. These studies often overlook changes in the local microclimate and incident solar radiation caused by reversing the exterior-corridor orientation. Although Pitts et al. [19] demonstrated that transition spaces can provide a significant thermal buffering effect during actual building operation, existing building performance evaluation models rarely treat the exterior corridor as an asymmetric climatic buffer whose effect varies with orientation. Consequently, the specific mechanism by which the exterior corridor, as a climatic buffer, regulates building cooling energy consumption remains unclear.

For the synergistic optimization of daylighting and energy consumption, previous studies have applied multi-objective optimization methods. Zhang et al. [20] developed a building-form optimization framework for school buildings using Non-dominated Sorting Genetic Algorithm II (NSGA-II) and other multi-objective genetic algorithms, with thermal comfort and daylighting performance considered simultaneously. Al-Masrani et al. [21] integrated daylighting metrics such as UDI with energy models to evaluate the nonlinear effects of shading-device geometry and louver angle on the indoor daylighting and thermal environment. Troup et al. [22] conducted empirical and optimization analyses of window-to-wall ratio and energy performance across different buildings and found that the optimal window proportion for achieving good daylighting with low cooling energy consumption often lies within a very narrow threshold range. Related studies have also applied multi-objective optimization to school classrooms and building envelopes by jointly considering energy and daylighting performance [23,24]. However, most existing studies treat buildings as homogeneous systems and perform building-level multi-objective optimization of passive design strategies, with limited attention to differences in climatic response among façades and orientations. In studies of teaching buildings with exterior corridors, different corridor orientations and the resulting heterogeneous design strategies have rarely been classified. Most optimization frameworks also overlook the orientation-dependent performance differences introduced by the exterior corridor as an asymmetric spatial component of the building [13,14]. As a result, the derived optimization strategies often lack spatial specificity when applied to practical design.

Machine learning techniques have been widely applied to the evaluation and prediction of building daylighting and energy performance [25–27]. For example, Tsanas and Xifara [28] used statistical machine learning algorithms, including Random Forest, to establish nonlinear mappings between building morphological parameters and cooling loads. Amasyali and El-Gohary [29] systematically reviewed state-of-the-art applications of data-driven models for building energy prediction and showed the potential of machine learning to model complex nonlinear relationships with high accuracy.

However, most related studies have used machine learning models for regression-based prediction of daylighting and thermal performance metrics. As Westermann and Evins [30] pointed out, these regression models essentially serve as surrogate models for physics-based simulation software, with their main contribution being to accelerate the simulation process and improve efficiency during the simulation stage. Machine learning models also often exhibit limited generalization when dealing with high-dimensional building design parameters and interpreting the trade-offs between daylighting and thermal performance [31,32]. During the early design stage, architects often need to quickly determine whether a design falls within a “high-performance region”, namely, one that simultaneously achieves high sDA, high UDI, and low cooling energy consumption intensity (Ec), rather than obtain an exact prediction of a specific performance value [33,34].

In addition, most existing surrogate models have a "black-box" nature and lack transparency [35]. Previous studies have indicated that conventional models have difficulty directly identifying the direction in which individual design variables contribute to overall performance [36].

Guangzhou is in China's hot-summer and warm-winter region, with long, hot, humid summers and building energy demand dominated by cooling. University teaching buildings have relatively high occupant densities and must also maintain adequate indoor daylight, creating a direct trade-off between controlling solar heat gain and using daylight. The linear teaching buildings with exterior corridors common on Guangzhou campuses are spatially asymmetric. With a north-facing corridor, the main exterior classroom windows face south and receive more direct solar radiation. With a south-facing corridor, the corridor itself provides deeper horizontal shading, while the main exterior windows face north and depend more on diffuse skylight. Reversing the corridor orientation may therefore change not only radiation and shading conditions, but also the distribution of favorable design parameters and the trade-off between daylighting and cooling energy use.

1.2. Research Gaps and Contributions

Previous research has established that orientation, fenestration, and shading affect building daylighting and energy performance. For teaching buildings with spatially asymmetric exterior corridors, however, a more specific question remains: when the corridor is moved from one side of the building to the other while other simulation and operational conditions remain unchanged, do the design-parameter distributions and priorities associated with high-performance solutions remain stable? Orientation has often been treated as a single design variable; fewer studies have compared whether reversing the corridor position reorganizes the high-performance design space as a whole.

Accordingly, this study does not seek simply to demonstrate that orientation affects performance. Instead, it compares the Pareto solution sets obtained for north- and south-facing corridor prototypes under the same design variables, weather conditions, and performance objectives. It asks whether the parameter distributions of high-performance solutions change and whether the ranking of parameter contributions to overall high-performance classification remains consistent. Machine-learning classification is used to turn the optimization results into rapid screening information for early-stage design, not to replace physics-based building simulation.

The contributions of this study are threefold. First, under the same weather, operating, design-variable, and optimization settings, this study compares favorable parameter combinations and the associated daylighting and cooling performance of north- and south-facing exterior corridors. Selected solutions are evaluated against a common baseline.

Second, the study examines whether moving the corridor from the north side to the south changes the contribution of the same design variables to high-performance classification. Model explanations are used to compare the magnitude and direction of predictive feature contributions, rather than establish causal effects on individual physical performance measures.

Third, orientation-specific classification models are evaluated for preliminary screening of teaching-building schemes in Guangzhou. These models are intended to inform parameter selection within the sampled design domain and do not replace physics-based daylighting or energy simulations.

2. Method

2.1. Integrated Research Framework

This study focused on teaching buildings with exterior corridors in Guangzhou and developed an integrated framework combining parametric simulation, multi-objective optimization, and machine learning classification. The framework comprised four sequential stages: parametric modeling, performance simulation, optimization, and classification evaluation, and was used to characterize the response patterns of daylighting and cooling energy consumption intensity under different spatial configurations (Figure 1).

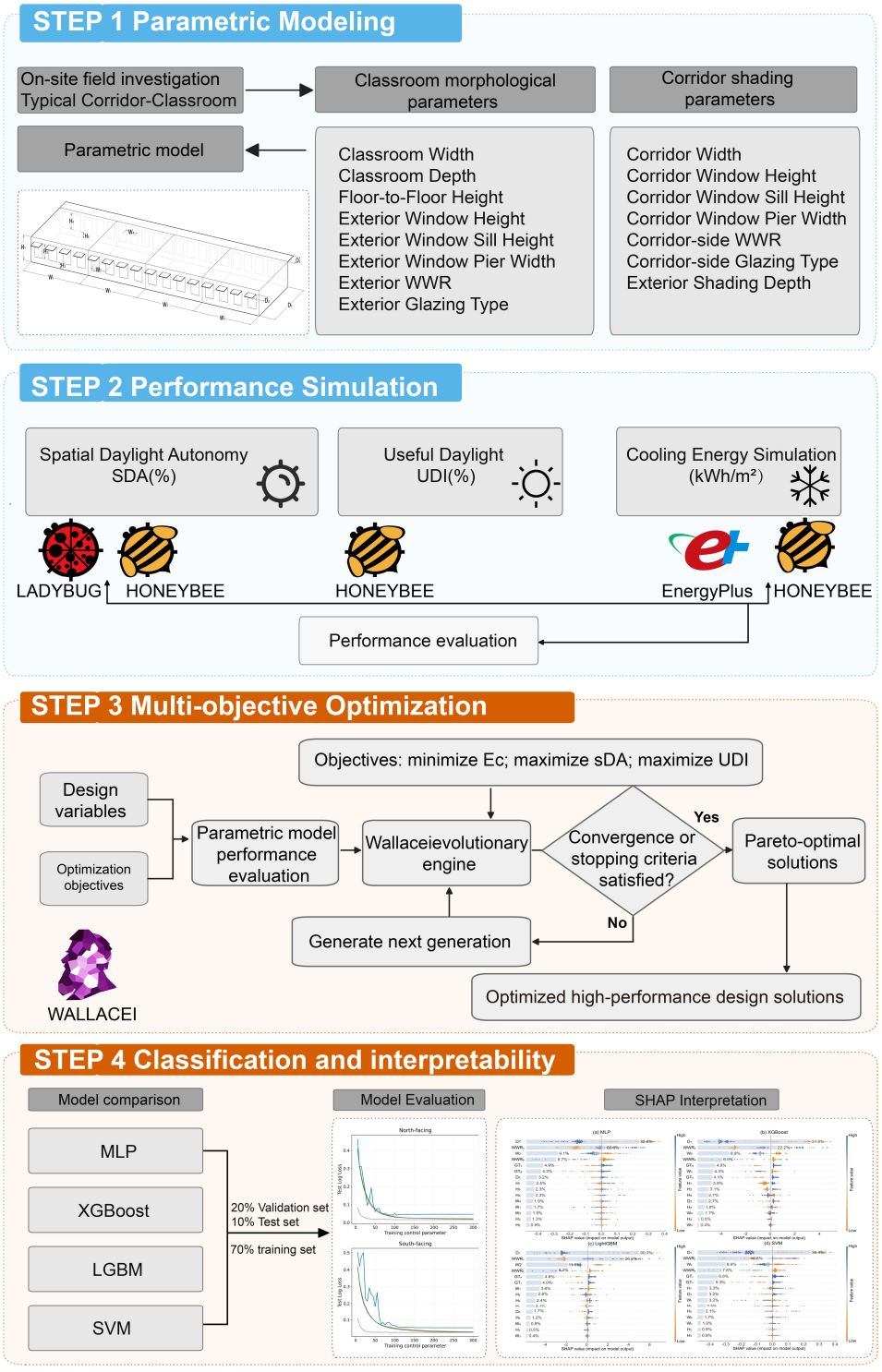

Figure 1. Research framework.

During the parametric modeling stage, a geometric model that could be iterated in batches was developed in Rhino 8 and Grasshopper (integrated with Rhino, version Rhino 8 based on the plan of a typical teaching building.Classroom depth, classroom width, exterior-corridor dimensions, window-to-wall ratios, shading devices, and building-envelope parameters were parameterized as decision variables, providing a diverse set of design alternatives for the subsequent multi-objective optimization.

Parametric geometry was developed in Rhino and Grasshopper. Building performance was simulated using Ladybug Tools and Honeybee [37,38], with Radiance for annual daylighting [39] and EnergyPlus for cooling-energy performance [40]. Multi-objective optimization was conducted with the Wallacei plugin for Grasshopper [41].

During the multi-objective optimization stage, cooling energy consumption intensity was minimized, while sDA and UDI were maximized. Multi-objective optimization was performed using the Wallacei plugin. After the Pareto-optimal solutions were obtained, the overall optimal solutions were used to compare the daylighting and thermal performance of the nondominated solutions under different spatial layouts, from which design schemes with better overall performance were selected. The favorable ranges of the design parameters within the Pareto-optimal solution sets were also analyzed to determine the corresponding parameter ranges for typical corridor models with different orientations.

Finally, a machine-learning classification model was developed to assess whether candidate schemes belong to the high-performance class defined by the combined score of the three performance metrics. SHapley Additive exPlanations (SHAP) were used to examine the contribution of each design variable to the class predictions and support preliminary design screening.

2.2. Field Survey and Parametric Model Development

Guangzhou has a hot-summer and warm-winter climate, with long, hot, humid summers and mild winters with low heating demand. Humidity and solar radiation are high, cooling dominates operational energy use, and solar heat gain must be balanced against daylight availability. From April to June 2025, 36 teaching buildings at 12 universities in Guangzhou were surveyed. On the basis of overall plan form, 28 were linear, five L-shaped, and three U-shaped. Linear buildings accounted for 77.8% (28/36), or approximately 78%, of this survey sample and were therefore selected as the main prototype for parametric modeling. This proportion describes only the buildings surveyed and should not be taken as the proportion of all university teaching buildings in Guangzhou. Fifteen ordinary classrooms in the linear buildings were then selected for detailed measurement. Selection focused on conventional teaching spaces with a clear classroom-corridor relationship; stepped lecture halls, laboratories, art studios, and other specialized rooms were excluded. Site observations, dimensional measurements, and photographs documented classroom dimensions, corridor width, fenestration, window-to-wall ratio, and shading geometry. These observations informed the design variables and ranges used in the subsequent Rhino-Grasshopper parametric model.

Field measurements were conducted in two classrooms located on the north and south sides of the same teaching building at a university in Guangzhou. The luminous and thermal environments of both classrooms were monitored. Air temperature and relative humidity were measured using a TES-1360A humidity/temperature meter (TES Electrical Electronic Corp., Taipei, Taiwan), while horizontal illuminance at desk level was measured using a TES-1339 light meter (TES Electrical Electronic Corp., Taipei, Taiwan). These variables were recorded from 08:00 to 18:00 at 15 min intervals. Measurement points were evenly distributed throughout each classroom at a workplane height of 0.75 m above

the floor. The layout of the measurement points and the on-site conditions are shown in Figure 2, while the instrument specifications are listed in Table 1.

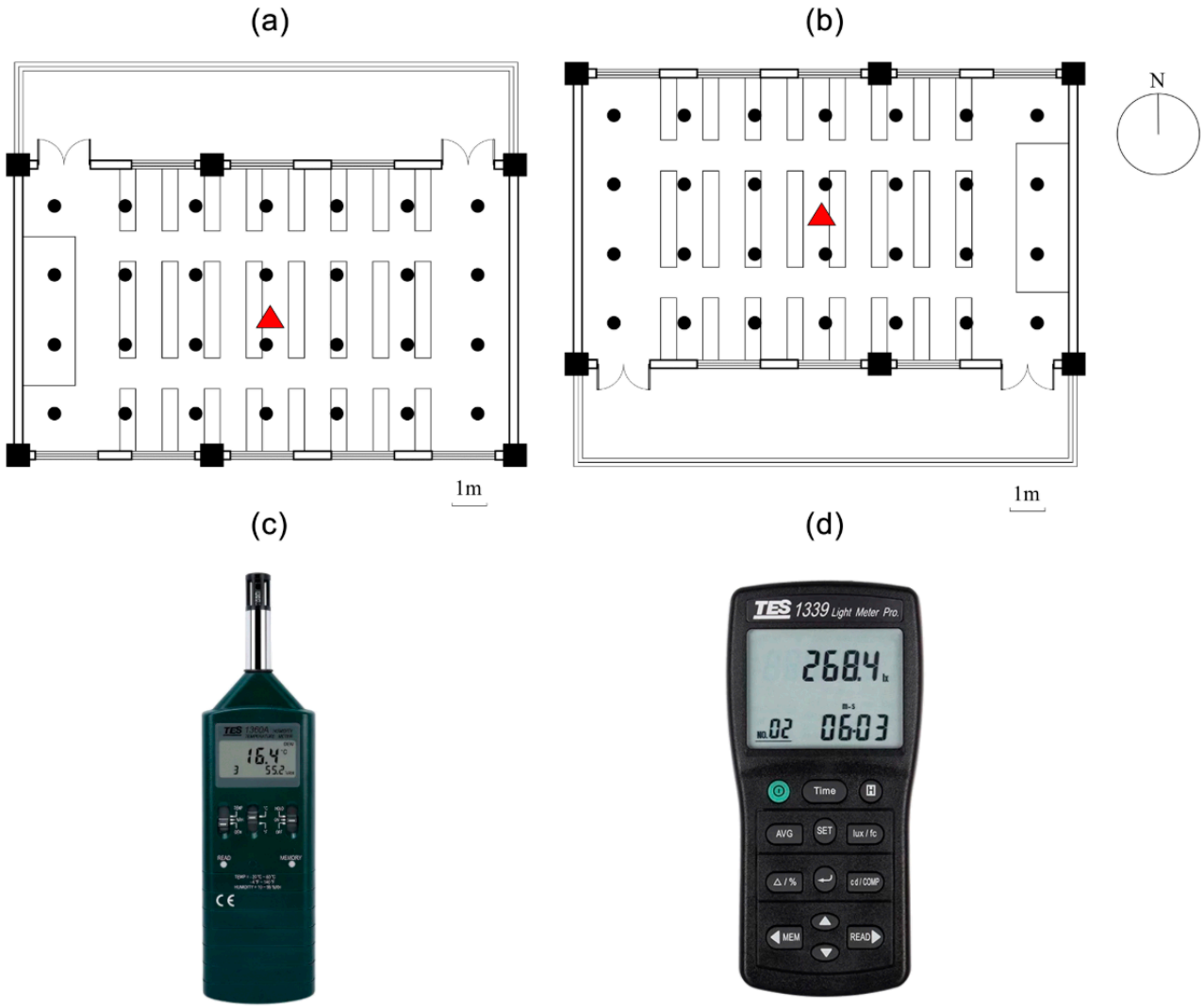

Figure 2. Layout of field measurement points and measurement instruments: (**a**) measurement-point layout in the classroom with a north-side exterior corridor; (**b**) measurement-point layout in the classroom with a south-side exterior corridor; (**c**) TES-1360A temperature and humidity meter; (**d**) TES-1339 illuminance meter. Red triangles indicate air temperature and relative humidity measurement locations, while black dots indicate illuminance measurement locations.

Table 1. Instrument specifications.

	Location	Equipment	Parameters	Test Time	Test Interval	Accuracy
Thermal test	Classroom (S) Classroom (N) Outdoor	TES-1360A	1. Temperature	8:00–18:00	15 min	±0.4 °C
			2. Humidity			±3%
Daylight test	Classroom (S) Classroom (N) Outdoor	TES-1339	Illuminance			±3%

The parametric model was built in Rhino-Grasshopper. The measured prototype had a single-storey linear block approximately 50 m long. To provide a consistent geometric

basis for comparison, this total building length was fixed for the baseline and all parametric cases. Classroom width (W_1) varied from 11.5 to 14.0 m as the classroom-unit width, while the overall building length remained unchanged. Classrooms on the same floor and their adjoining corridor were treated as one unit, described by 16 design variables. Figure 3 summarizes the parameter ranges, and Table 2 lists their units and increments. The main classroom façades of the surveyed linear-plan buildings were predominantly oriented north or south, and the field measurements were likewise conducted in ordinary classrooms on the north and south sides of the same building. To maintain consistency among the surveyed cases, prototype selection, and subsequent optimization, the current comparison was limited to 0° and 180°, representing the principal north- and south-facing classroom and corridor configurations. East- and west-facing cases were not included in the present optimization and will be examined in a subsequent four-orientation study.

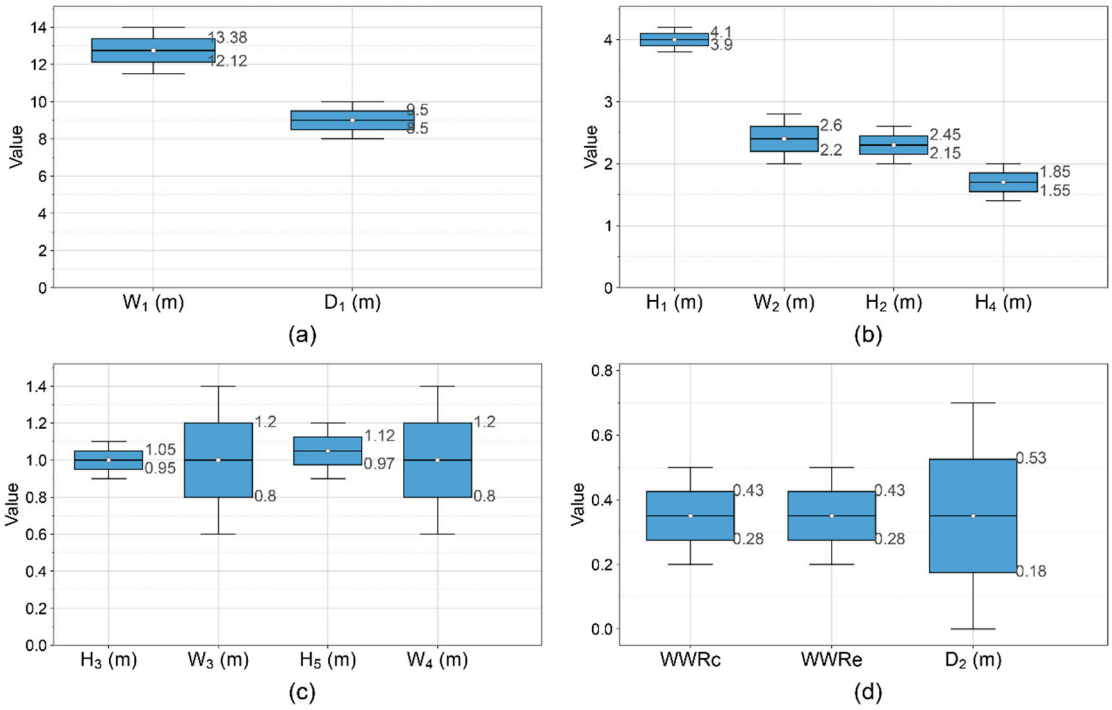

Figure 3. Distribution of design parameters for the surveyed classrooms and exterior-corridor shading systems: (**a**) classroom width (W_1) and classroom depth (D_1); (**b**) floor height (H_1), corridor width (W_2), exterior window height (H_2), and corridor window height (H_4); (**c**) exterior window sill height (H_3), exterior window pier width (W_3), corridor window sill height (H_5), and corridor window pier width (W_4); (**d**) corridor-side window-to-wall ratio (WWR_c), exterior window-to-wall ratio (WWR_e), and exterior shading depth (D_2).

Exterior- and corridor-side window openings were generated separately after the walls. The corresponding window-to-wall ratios (WWR_e and WWR_c) determined the target total opening area on each wall; window heights (H_2 and H_4) and sill heights (H_3 and H_5) defined the vertical dimensions and positions, while window-pier widths (W_3 and W_4) set the horizontal spacing between adjacent openings. Window width was not an independent variable but was calculated from the target window-to-wall ratio, window height, and available wall length. The resulting rectangular openings were assigned to their walls as Honeybee Apertures. Infeasible combinations extending beyond wall boundaries or producing overlapping openings were excluded before performance simulation.

For the glazing properties, clear, heat-absorbing, and Low-E insulating glazing could be assigned separately to the exterior-window side and corridor side. The visible transmittance ranged from 0.68 to 0.81, the Solar Heat Gain Coefficient (SHGC) from 0.46 to

0.75, and the U-value from 1.72 to 2.60 $W \cdot m^{-2} \cdot K^{-1}$. The glazing constructions and thermal properties used in the parametric models are provided in Table 3. A parametric model was then developed using the parameters obtained from the field survey, as shown in Figure 4. Daylighting and thermal-environment simulations were subsequently performed to evaluate each parameter combination, and the simulation results were used in the multi-objective optimization experiments.

Table 2. The morphological design parameters of the parametric model for medium-sized classrooms.

Category	Design Parameter	Range	Unit	Step
Plan parameters	Classroom Width (W_1)	11.5–14.0	m	0.5
	Classroom Depth (D_1)	8.0–10.0	m	0.25
	Floor Height (H_1)	3.8–4.2	m	0.2
	Orientation (θ)	0, 180	°	180
	Corridor Width (W_2)	2.0–2.8	m	0.2
Façade parameters	Exterior Window Height (H_2)	2.0–2.6	m	0.2
	Exterior Window Sill Height (H_3)	0.9–1.1	m	0.1
	Exterior Window Pier Width (W_3)	0.6–1.4	m	0.2
	Corridor Window Height (H_4)	1.4–2.0	m	0.2
	Corridor Window Sill Height (H_5)	0.9–1.2	m	0.1
	Corridor Window Pier Width (W_4)	0.6–1.4	m	0.2
	Corridor-side Window-to-Wall Ratio (WWR_c)	0.20–0.50	—	0.05
	Exterior Window-to-Wall Ratio (WWR_e)	0.20–0.50	—	0.05
Thermal parameters	Exterior Glazing Type (GT_e)	0, 1, 2 (three types)	—	1
	Corridor-side Glazing Type (GT_c)	0, 1, 2 (three types)	—	1
	Exterior Shading Depth (D_2)	0–0.7	m	0.1

Table 3. Thermal properties of the opaque envelope and glazing configurations used in the simulation model.

Type	Envelope Component/ Glazing Option	Construction	Visible Transmittance	SHGC	U-Value [$W/(m^2 \cdot K)$]
Opaque	Exterior wall (aerated concrete)	—	—	—	0.70
	Roof (XPS insulation)	—	—	—	0.40
	Floor slab (reinforced concrete)	—	—	—	1.50
	Interior partition (aerated concrete)	—	—	—	1.50
0	Clear glass	6 mm clear glass + 12 mm air layer + 6 mm clear glass	0.81	0.75	2.59
1	Heat-absorbing glass	6 mm heat-absorbing glass + 12 mm air layer + 6 mm clear glass	0.68	0.49	2.60
2	Low-E glass	6 mm Low-E glass + 12 mm air gap + 6 mm clear glass	0.68	0.46	1.72

In addition to glazing, the same opaque-envelope U-values were used for both corridor orientations. The U-values of the exterior wall, roof, floor slab, and interior partition were 0.70, 0.40, 1.50, and 1.50 $W/(m^2 \cdot K)$, respectively. These values were fixed energy-model inputs and were not included among the optimization variables.

In the daylight model, visible reflectance was set to 0.75 for the ceiling and interior walls, and 0.50 for the floor, exterior corridor, and shading surfaces. In the energy model,

the exterior wall, classroom wall facing the corridor, and roof had Outdoors boundary conditions; the ground-floor slab had a Ground boundary condition; and partitions between adjacent conditioned classrooms had Surface boundary conditions. The open corridor was modeled as exterior shading geometry rather than a conditioned thermal zone.

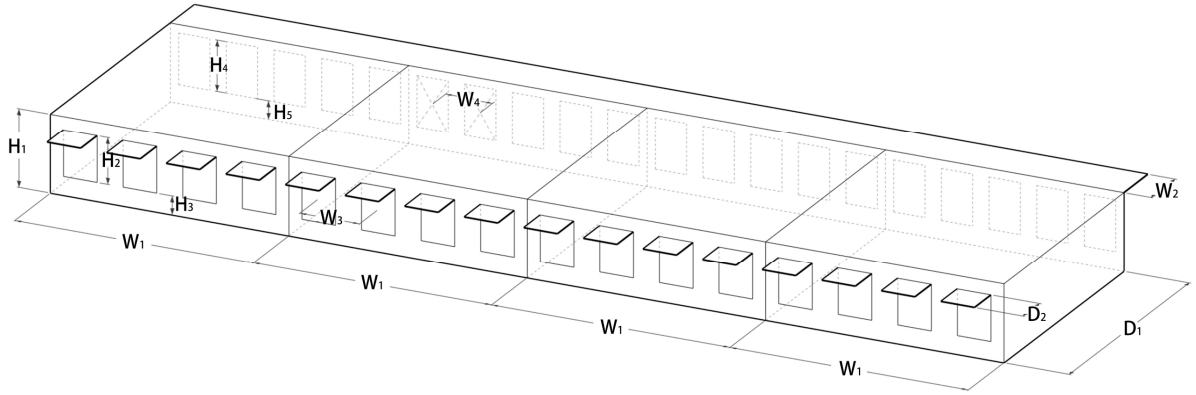

Figure 4. Parametric model prototype. (Solid lines represent visible geometric edges, while dashed lines indicate hidden edges of building components).

Occupancy, lighting, and equipment settings were used to define internal heat gains in the energy model. In accordance with the Design Standard for Energy Efficiency of Public Buildings (GB 50189-2015) [42]. The settings for internal heat gains, including occupant density, lighting power density, and equipment power density, together with the intermittent operation schedules, were summarized in Table 4. The simulations were driven by typical meteorological year (TMY) weather data for Guangzhou, providing a high-fidelity and quantifiable computational basis for the subsequent multi-objective optimization.

Table 4. Parameter settings for occupants and equipment.

Parameter	Setting
Simulation Period	1 January to 31 December
Occupancy Schedule	Monday to Friday: 8:00–18:00 Saturday to Sunday: Closed Holiday: Closed
Occupant density (m^2/person)	1.5
Lighting Power Density (W/m^2)	9
Equipment Power Density (W/m^2)	5
Room summer setpoint temperature (°C)	26
Room winter setpoint temperature (°C)	18
Fresh air volume [m^3/(h·person)]	30
Cooling COP (constant)	5.6
Test grid size (m)	2 m × 2 m
Illuminance sensor height (m)	0.75
Intensity of infiltration	0.0003 $m^3/(s \cdot m^2)$

A fixed cooling coefficient of performance (COP) of 5.6 was used to represent air-conditioning efficiency in the energy model and was held constant across all parametric designs.

Annual daylight simulations used the Honeybee-Radiance enhanced two-phase method and hourly typical-meteorological-year data for Guangzhou. Radiance settings were -ab 2 -ad 5000 -lw 2×10^{-5}. A sensor point contributed to spatial daylight autonomy when illuminance was at least 300 lx for at least 50% of occupied hours; useful daylight illuminance was calculated for illuminance from 100 to 2000 lx. The sensor grid spacing

was 2 m × 2 m at a workplane height of 0.75 m, and annual metrics were evaluated during occupied weekday hours from 08:00 to 18:00.

2.3. Performance Metrics and Multi-Objective Optimization

Daylighting conditions in Guangzhou vary throughout the year with solar geometry, cloud conditions, and building façade orientation. Illuminance at a single point in time therefore cannot adequately represent the annual daylighting performance of classrooms. In this study, spatial daylight autonomy (sDA) was used to evaluate daylight availability on the work plane 0.75 m above the floor [43,44]. It is defined as:

$$\mathrm{sDA}_{300/50\%} = \frac{1}{N}\sum_{i=1}^{N} I\left(\frac{1}{T}\sum_{t=1}^{T} I(E_{i,t} \geq 300) \geq 0.5\right) \quad (1)$$

where E_i,t is the illuminance at sensor i and time t (lx); N is the total number of workplane sensors; T is the number of occupied time steps in the year; and I(·) is an indicator function taking a value of 0 or 1. N, T, and I(·) have no physical units. The illuminance threshold is 300 lx and the time-fraction threshold is 0.5. sDA is dimensionless and is reported as a proportion between 0 and 1.

sDA cannot distinguish between useful daylight and excessive glare. Useful Daylight Illuminance (UDI) was therefore introduced to evaluate the proportion of occupied hours during the year for which illuminance remains within a comfortable range [45]. It is expressed as:

$$UDI_{100-2000} = \frac{n_{100-2000}}{N\,T} \quad (2)$$

where the corresponding term denotes the total sensor-point hours during annual occupied periods for which illuminance falls within the range of 100 to 2000 lx, and the remaining terms are as defined above. Illuminance below 100 lx indicates insufficient daylight, whereas illuminance above 2000 lx may cause visual discomfort.

Guangzhou is in China's hot-summer and warm-winter region, where summer solar radiation is strong and prolonged, winters are mild, and heating demand is low; operational energy demand is therefore dominated by cooling. The field survey further indicated that the teaching buildings studied did not use continuous space heating during typical winter operation, so heating energy use was not included among the optimization objectives. If heating were considered, winter solar gains might offset part of the heating load and alter the trade-offs associated with shading, window openings, and glazing; this effect is outside the scope of the present study. Building orientation and facade design affect solar heat gain and cooling loads. Cooling was therefore selected as the thermal-performance optimization metric. For all designs, the annual cooling load was converted to cooling electricity use using a fixed COP of 5.6. Cooling Energy Consumption Intensity is defined as follows:

$$Ec = \frac{E}{A} \quad (3)$$

where E is annual cooling electricity use converted using the fixed COP of 5.6 (kWh), A is conditioned floor area (m^2), and Ec is cooling energy consumption intensity (kWh/m^2). The same COP was applied to all designs so that differences in equipment efficiency would not affect their comparison. Ec was minimized in the multi-objective optimization, while sDA and UDI were maximized.

Using these performance metrics, multi-objective optimization was then conducted to examine daylighting-cooling trade-offs across combinations of design variables.

The multi-objective optimization was conducted in Grasshopper using the Wallacei plugin, which performs Pareto-front-based evolutionary search with NSGA-II. The north-

corridor and south-corridor prototypes were optimized separately under the same design-variable ranges, material properties, weather data, and occupancy conditions. Each run used 40 individuals over 60 generations, with crossover and mutation probabilities of 0.90 and 0.05, respectively (Table 5). These settings were selected with reference to commonly used NSGA-II configurations in related building-performance optimization studies and were applied identically to both orientations. NSGA-II ranks candidate solutions through non-dominated sorting and crowding distance and generates offspring through selection, crossover, and mutation. The objective vector was expressed as follows:

$$\mathrm{F(x)} = \min\left\{\frac{1}{\mathrm{sDA(x)}}, \frac{1}{\mathrm{UDI(x)}}, \mathrm{Ec(x)}\right\} \tag{4}$$

where x is the design-variable vector (variable units are given in Table 2); sDA(x) and UDI(x), and thus their reciprocals 1/sDA(x) and 1/UDI(x), are dimensionless; and Ec(x) is the cooling energy consumption intensity to be minimized (kWh/m^2).

Table 5. Parameter settings of the genetic algorithm.

Parameter	Generation Size	Generation Count	Crossover Probability	Mutation Probability	Random Seed
Value	40	60	0.90	0.05	1

2.4. Classification Modeling and Interpretability Analysis

For dataset construction, the historical solution sets from the multi-objective optimization experiments were processed separately for the north-facing and south-facing corridor cases. Each orientation contained 2400 design schemes. To remove dimensional differences, UDI, sDA, and cooling energy consumption intensity (Ec) were normalized using Min-Max normalization. UDI and sDA were normalized in the positive direction, whereas Ec was reverse normalized. The three normalized indicators were then assigned equal weights, and their arithmetic mean was used as the comprehensive performance score. For each orientation, the dataset was sorted in descending order according to this score. The top 25%, corresponding to 600 schemes, was defined as the high-performance class and labeled as 1, while the remaining 1800 schemes were labeled as 0. The labeled datasets were then used to construct the subsequent classification models.

$$y_i = I\left(\frac{UDI_i^* + sDA_i^* + Ec_i^*}{3} \geq T_{75}\right) \tag{5}$$

where UDI_i, sDA_i, and Ec_i are normalized performance indicators between 0 and 1 and have no physical units; T_75 is the dimensionless 75th-percentile threshold of the overall performance score; y_i is a dimensionless binary class label taking a value of 0 or 1; and $I(\cdot)$ is a dimensionless indicator function.

Based on the labelled classroom design dataset, four supervised classification models were constructed. Extreme Gradient Boosting (XGBoost) [46] learns by sequentially adding decision trees, with each subsequent tree correcting the residual errors left by previous learners. Light Gradient Boosting Machine (LightGBM) [47] also follows a gradient boosting strategy. It combines histogram-based feature discretization with a leaf-wise growth strategy to organize the splitting of predictor variables efficiently during classification.

Support Vector Machine (SVM) [48] determines the classification hyperplane by maximizing the margin between support vectors and uses kernel functions, when needed, to obtain more flexible class boundaries. The Multilayer Perceptron (MLP) [49] feeds the design variables into hidden layers, passes them through activation functions layer by

layer, and updates the connection weights through backpropagation. The four models were compared under the same dataset conditions. This setup provided a consistent basis for the subsequent evaluation of classification performance and the analysis of individual design-variable contributions.

For each corridor orientation, the labeled dataset was divided into training, validation, and independent test sets in proportions of 70%, 20%, and 10%, respectively. The training set was used to learn model parameters and the validation set to select models and tune hyperparameters. Once the model configuration was fixed, the independent test set was used only for final evaluation. After reserving the test set, stratified five-fold cross-validation was additionally conducted on the model-development data to examine internal classification stability, and Precision, Recall, and F1-score were summarized as mean ± standard deviation across folds.

Precision, Recall, and F1-score were used to evaluate the performance of the classification models. Precision [50] denotes the proportion of samples predicted by the model as high-performance design solutions that were correctly classified. Recall [51] denotes the proportion of actual high-performance design solutions that were correctly identified by the model. F1-score [52] is the harmonic mean of Precision and Recall, and was used to describe the balance between false positives and false negatives. The three metrics are defined as follows:

$$Precision = \frac{TP}{TP + FP} \tag{6}$$

$$Recall = \frac{TP}{TP + FN} \tag{7}$$

$$F1\text{-score} = \frac{2 \times Precision \times Recall}{Precision + Recall} \tag{8}$$

where TP is the number of high-performance designs correctly identified as positive, FP is the number of lower-performance designs incorrectly identified as high-performance, and FN is the number of high-performance designs incorrectly identified as lower-performance. TP, FP, and FN are sample counts without physical units; Precision, Recall, and F1-score are dimensionless metrics.

Machine learning models have strong feature extraction and nonlinear fitting capabilities. However, their internal structures often have a black-box nature, making it difficult to explain how individual design variables contribute to the prediction results. To address this issue, this study applied SHapley Additive exPlanations (SHAP) [53]. SHAP is derived from cooperative game theory and calculates the marginal contribution of each feature i to the model prediction. It is defined as follows:

$$\phi_i = \sum_{S \subseteq N \setminus \{i\}} \frac{|S|!(|N| - |S| - 1)!}{|N|!} [v(S \cup \{i\}) - v(S)] \tag{9}$$

where N is the set of all input features, S is a feature subset, and |N| and |S| are the respective numbers of features (dimensionless counts). v(·) is the classifier output used by the SHAP explainer and has no building-physics unit; the SHAP value phi_i for feature i is on the same output scale as v(·). Global feature importance was ranked by the mean absolute SHAP value of each variable.

3. Results

3.1. Field Measurements and Model Validation

The field measurements showed clear differences in the daylighting and thermal environments between classrooms with different orientations (Figure 5). During most of the monitoring period, indoor illuminance was higher in the south-facing classroom than

in the north-facing classroom. Both classrooms reached their peak illuminance around noon, at approximately 500 lx for the south-facing classroom and 400 lx for the north-facing classroom, after which illuminance gradually decreased. Air temperature showed a similar diurnal pattern. The south-facing classroom generally had a higher indoor temperature, with a peak of 27.5 °C. The north-facing classroom reached a lower peak temperature of 25.5 °C and exhibited smaller fluctuations during the daytime. On the basis of these field measurements, the parametric simulation workflow was validated against data from the same classrooms under the corresponding boundary conditions.

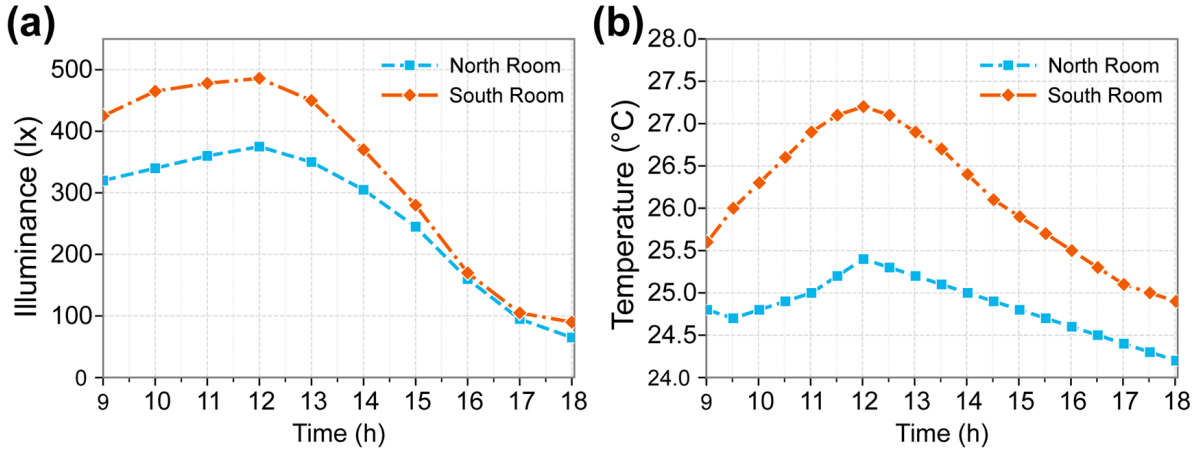

Figure 5. Comparison of measured indoor illuminance and air temperature in the south- and north-facing classrooms: (**a**) horizontal indoor illuminance; (**b**) indoor air temperature.

Before conducting the multi-objective optimization, the accuracy of the simulation workflow was first validated. Parametric models were established based on the classrooms investigated in the field, with the measured illuminance and temperature data used as reference values. Radiance and Honeybee were then used to simulate daylighting and thermal performance, and SPSSPRO was used to conduct correlation and significance tests between the simulated and measured values to quantify the accuracy of the simulation results.The simulations reproduced the daytime variation trends of the two classroom orientations well under the same calibration boundary conditions. Figure 6 and Table 6 present the curve-fitting results and error evaluation between the measured and simulated daylighting and thermal performance data. The coefficient of determination (R^2) values for the illuminance simulations of the north- and south-facing classrooms are 0.944 and 0.936, respectively; the corresponding values for the temperature simulations are 0.934 and 0.929 (Table 6). The reported agreement supported the use of the simulation workflow in the subsequent optimization under the tested conditions.

Table 6. Coefficient of determination (R^2) and mean absolute percentage error (MAPE) values for illuminance and temperature under north- and south-facing orientations.

Orientation	Variable	R^2	MAPE
North	Illuminance (lx)	0.944	13.21%
	Temperature (°C)	0.934	0.30%
South	Illuminance (lx)	0.936	13.76%
	Temperature (°C)	0.929	0.65%

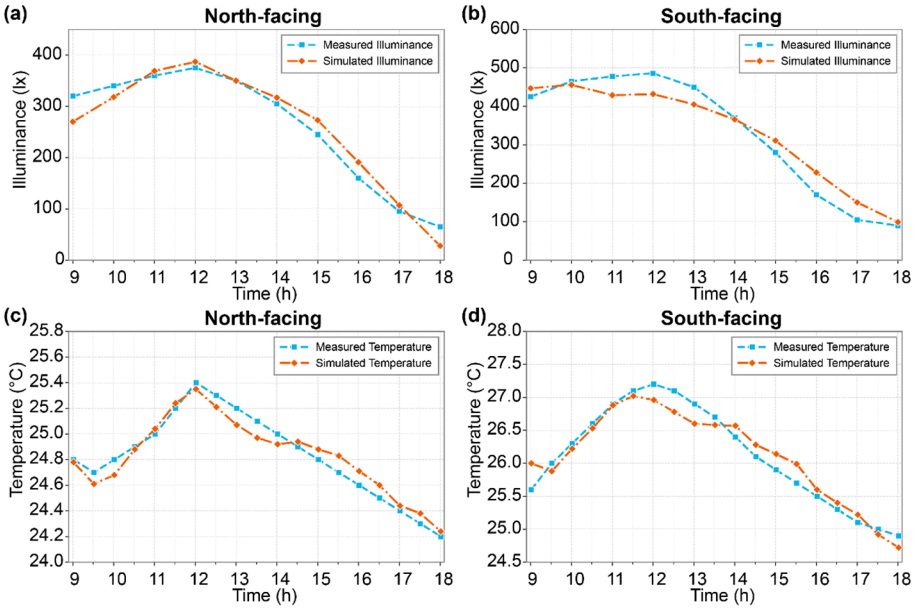

Figure 6. Comparison of measured and simulated indoor illuminance and air temperature for the north- and south-facing classrooms: (**a**) indoor illuminance in the north-facing classroom; (**b**) indoor illuminance in the south-facing classroom; (**c**) air temperature in the north-facing classroom; (**d**) air temperature in the south-facing classroom.

3.2. Analysis of Multi-Objective Optimization Results

The distributions of design parameters in the Pareto-optimal solution sets differed between the two corridor orientations. In plan, Figure 7a shows that classroom depth (D_1) in the south-facing-corridor model, whose exterior windows face north and rely mainly on diffuse skylight, was concentrated at 8.5–9.0 m. In the north-facing-corridor model, whose exterior windows face south and receive direct sunlight, D_1 extended to 8.5–10.0 m. The lower illuminance available at north-facing windows may explain this difference: a shallower classroom shortens the distance daylight must travel and reduces the poorly lit area. Consequently, the south-facing-corridor model could maintain relatively high sDA and UDI without a substantial increase in exterior glazing area. The south-facing exterior windows of the north-facing-corridor model receive more direct sunlight, allowing a deeper classroom without a marked reduction in daylighting performance. Corridor width (W_2) also differed by orientation (Figure 7b): values were 2.6–2.8 m for the south-facing corridor and 2.2–2.6 m for the north-facing corridor. A wider south-facing corridor projects farther outward and increases its self-shaded area, intercepting direct solar radiation before it reaches the classroom glazing and thereby reducing Ec. Limiting excessive direct light may also reduce near-window glare and place more illuminance within the 100–2000 lx UDI interval, improving the balance between daylighting and thermal performance.

Figure 7c–f summarize the façade parameters. Exterior Window Height (H_2) and Exterior Window Sill Height (H_3) in the north-facing-corridor model were mainly 2.0–2.2 m and 1.0–1.1 m, respectively, whereas both were concentrated at 2.0 m and 1.1 m in the south-facing-corridor model. For both orientations, Corridor Window Height (H_4) and Corridor Window Sill Height (H_5) were mainly 1.8–2.0 m and 0.9–1.0 m. The exterior window-to-wall ratio (WWR_e) reached 0.20 for both corridor orientations. By contrast, corridor-side window-to-wall ratio (WWR_c) and Corridor Window Pier Width (W_4) differed between orientations. For the north-facing corridor, W_4 ranged from 0.8 to 1.2 m and the lower bound of WWR_c was 0.25. For the south-facing corridor, W_4 was concentrated at 1.0 m and the lower bound of WWR_c was 0.30.

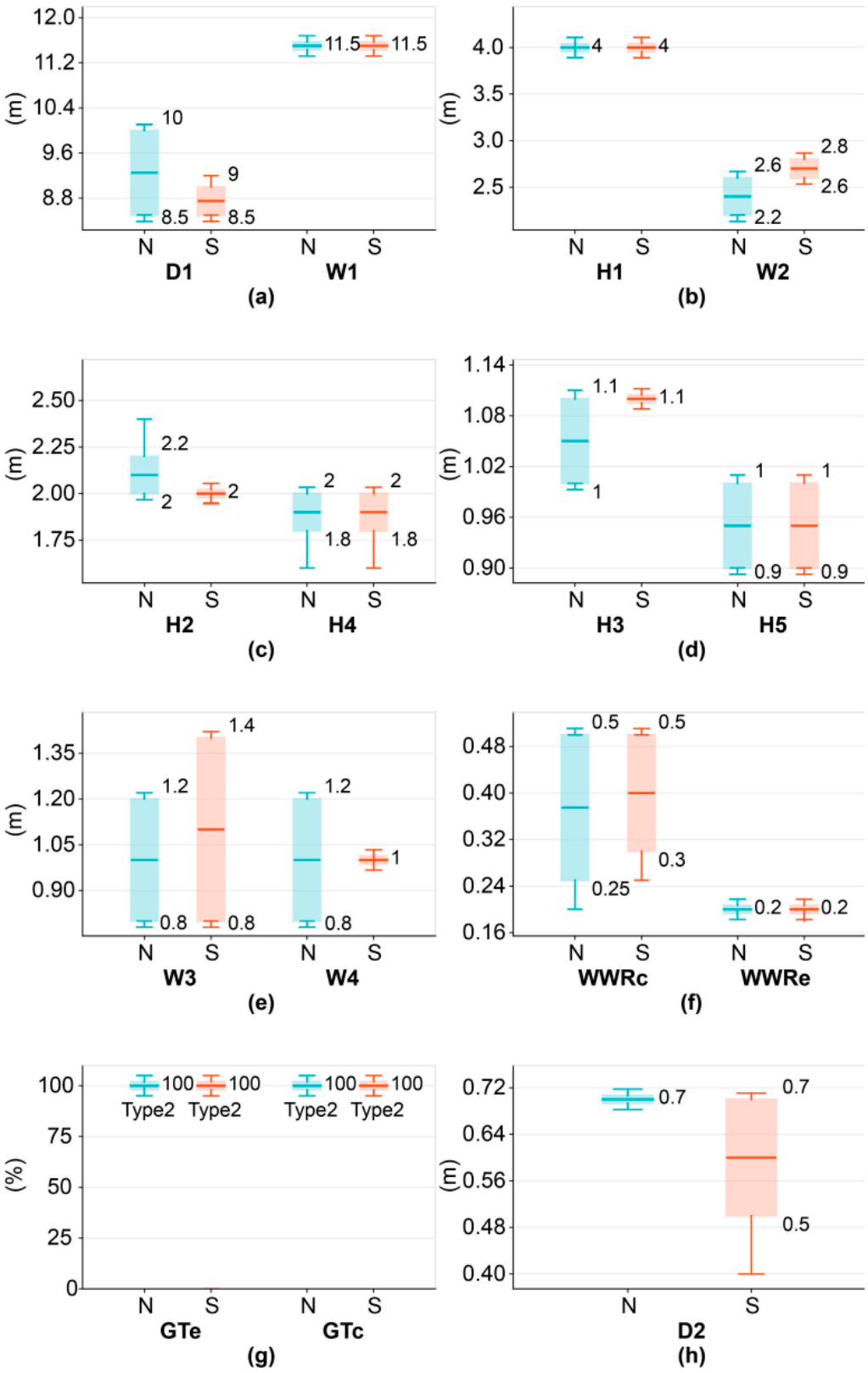

Figure 7. Distribution of design parameters in the optimized solution sets for the two corridor orientations: (**a**) classroom depth (D_1) and width (W_1); (**b**) floor height (H_1) and corridor width (W_2); (**c**) exterior window height (H_2) and corridor window height (H_4); (**d**) exterior window sill height (H_3) and corridor window sill height (H_5); (**e**) exterior window pier width (W_3) and corridor window pier width (W_4); (**f**) corridor-side window-to-wall ratio (WWR_c) and exterior window-to-wall ratio (WWR_e); (**g**) exterior glazing type (GT_e) and corridor-side glazing type (GT_c); and (**h**) exterior shading depth (D_2).

Compared with the geometric parameters, the thermal parameters showed stronger convergence. As shown in Figure 7g, both the Exterior Glazing Type (GT_e) and Corridor-side Glazing Type (GT_c) converged completely to Type 2 under both corridor orientations. This Low-E glazing has a visible light transmittance of 0.68, a solar heat gain coefficient (SHGC) of 0.46, and a U-value of 1.72 W/(m^2·K). It can maintain a certain level of daylight transmission while limiting solar heat gain.

The façade-parameter distributions therefore show that the two corridor configurations differ not only in corridor width but also in the opening arrangement on the corridor side.

Figure 7h shows that exterior shading depth (D_2) was mainly 0.7 m for the north-facing-corridor model, while the south-facing-corridor model had a wider observed range of 0.5–0.7 m.

Following this comparison of parameter distributions, representative solutions for the different optimization objectives were selected to compare their design parameters and performance. Four representative types of solutions were selected from the history solution set for each corridor orientation. sDA-Max and UDI-Max correspond to the maximum values of Spatial Daylight Autonomy and Useful Daylight Illuminance, respectively, while Ec-Min represents the solution with the lowest cooling energy consumption intensity. The solution with the highest multi-criteria decision-making score was defined as the overall optimal solution. By tracing the parameter combinations of these representative solutions, the relationships between different optimization objectives and spatial configuration, fenestration, shading, and glazing configuration can be further identified.

The north-facing corridor model exhibited a clear trade-off between daylighting and thermal performance (Figure 8). As shown in Table 7, the sDA-Max solution adopts a relatively small classroom depth (D_1 = 8.0 m) and an exterior WWR (WWR_e) of 0.35. The larger exterior WWR increases sDA to 0.906, but the associated solar heat gain raises Ec sharply to 37.31 kWh/m^2. This result indicates that the improvement in daylighting performance is achieved at the expense of energy performance. For the UDI-Max solution, the exterior shading depth (D_2) is increased to 0.70 m while WWR_e is maintained at a relatively low level of 0.20. The deeper exterior shading limits direct sunlight that may contribute to glare, resulting in a UDI of 0.826 while keeping Ec at 33.27 kWh/m^2, thereby improving the coordination between daylighting and thermal performance. In contrast, the Ec-Min solution increases the classroom depth (D_1) to 10.0 m and reduces the corridor-side WWR (WWR_c) to 0.20 to limit solar heat gain. Although Ec decreases to 25.57 kWh/m^2, sDA and UDI fall to 0.430 and 0.371, respectively, indicating that the improvement in energy performance is achieved at the expense of daylighting.

The overall optimal solution for the north-facing-corridor model achieves an sDA of 0.856, a UDI of 0.790, and an Ec of 29.23 kWh/m^2, showing coordinated improvement in daylighting and thermal performance. In this solution, D_1 is set to 8.5 m, together with a corridor-side WWR (WWR_c) of 0.50 to maintain diffuse daylight penetration and compensate for illuminance attenuation in deeper areas of the classroom. At the same time, the exterior window proportion is strictly controlled to limit heat gain, resulting in a more favorable balance between daylighting and thermal performance.

For the south-facing corridor model, the parameter responses show a different pattern, as presented in Table 8 and Figure 9. Owing to the self-shading effect of the exterior corridor, both the sDA-Max and UDI-Max solutions maintain a high Corridor-side WWR (WWR_c = 0.50), combined with an Exterior Shading Depth (D_2) of 0.70 m. Under this configuration, the shading limits excessive illuminance that may cause visual discomfort, increasing UDI to 0.746 while maintaining Ec at approximately 30.8 kWh/m^2. The Ec-Min solution controls heat gain by increasing Classroom Depth (D_1) to 9.0 m and reducing the Corridor-side WWR (WWR_c) to 0.25. Although Ec decreases to 24.34 kWh/m^2, sDA drops sharply to 0.588, indicating that the lower energy consumption is accompanied by a

substantial reduction in spatial daylight autonomy. The overall optimal solution for the south-facing corridor achieves an sDA of 0.820, a UDI of 0.711, and an Ec of 26.88 kWh/m^2, consistent with an important role for passive shading in this orientation. Specifically, Corridor Width (W_2) is increased to 2.8 m to exploit the shading effect provided by the wider corridor projection, together with an Exterior Shading Depth (D_2) of 0.60 m. Meanwhile, a relatively high Corridor-side WWR (WWR_c) is retained to supplement daylight while solar heat gain is minimized. This combination results in a relatively favorable balance between daylighting and thermal performance.

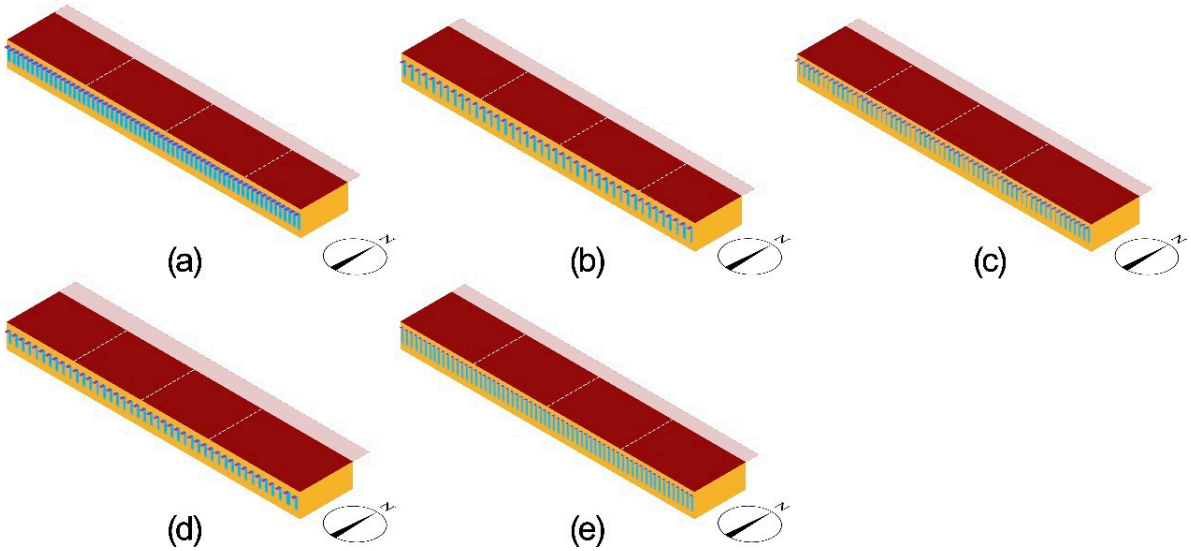

Figure 8. Parametric models of five design configurations for the north-facing corridor case: (**a**) sDA-Max solution, (**b**) UDI-Max solution, (**c**) Ec-Min solution, (**d**) overall optimal solution, and (**e**) baseline model. In the rendered building models, dark red surfaces represent roofs, yellow surfaces represent opaque walls, and blue surfaces represent window glazing.

Table 7. Design parameters and performance metrics of representative design solutions selected from the optimization history and the corresponding baseline model for the north-facing corridor.

Dimension	Parameter	sDA-Max	UDI-Max	Ec-Min	Overall Optimal	Baseline Model
Spatial Morphology	D_1 (m)	8	8	10	8.5	8.75
	W_1 (m)	13.5	13.5	11.5	11.5	12.5
	H_1 (m)	4.2	4.2	4	4	4
	W_2 (m)	2.2	2.2	2.8	2.2	2.2
	D_2 (m)	0.7	0.7	0.7	0.7	0.3
	H_2 (m)	2.4	2.4	2	2.4	2.4
	H_3 (m)	1.1	1	1.1	1.1	1
	W_3 (m)	0.8	1.2	1.2	0.8	0.8
	H_4 (m)	1.8	1.8	2	1.8	1.6
	H_5 (m)	0.9	0.9	1	1	1
	W_4 (m)	0.8	1	1.2	1.2	1
	WWR_c	0.5	0.5	0.2	0.5	0.3
	WWR_e	0.35	0.2	0.2	0.2	0.25
Thermal Configuration	GT_e	Type-2	Type-2	Type-2	Type-2	Type-1
	GT_c	Type-2	Type-2	Type-2	Type-2	Type-1
Performance Metrics	sDA	0.906	0.884	0.430	0.856	0.752
	UDI	0.800	0.826	0.371	0.790	0.693
	Ec (kWh/m^2)	37.31	33.27	25.57	29.23	33.35

Table 8. Design parameters and performance metrics of representative design solutions selected from the optimization history and the corresponding baseline model for the south-facing corridor.

Dimension	Parameter	sDA-Max	UDI-Max	Ec-Min	Overall Optimal	Baseline Model
Spatial Morphology	D_1 (m)	8.25	8.25	9	8.5	8.75
	W_1 (m)	14	14	11.5	11.5	12.5
	H_1 (m)	4.2	4.2	3.8	4	4
	W_2 (m)	2.6	2.6	2.6	2.8	2.2
	D_2 (m)	0.7	0.7	0.7	0.6	0.3
	H_2 (m)	2	2	2	2	2.4
	H_3 (m)	1.1	1.1	1.1	1.1	1
	W_3 (m)	1.4	0.8	1.4	1.4	0.8
	H_4 (m)	2	2	1.8	2	1.6
	H_5 (m)	0.9	0.9	1	0.9	1
	W_4 (m)	1	1	1.2	1	1
	WWR_c	0.5	0.5	0.25	0.5	0.3
	WWR_e	0.2	0.2	0.2	0.2	0.25
Glazing Configuration	GT_e	Type-0	Type-0	Type-2	Type-2	Type-1
	GT_c	Type-2	Type-2	Type-2	Type-2	Type-1
Performance Metrics	sDA	0.883	0.883	0.588	0.820	0.752
	UDI	0.740	0.746	0.422	0.711	0.693
	Ec (kWh/m^2)	30.83	30.86	24.34	26.88	33.35

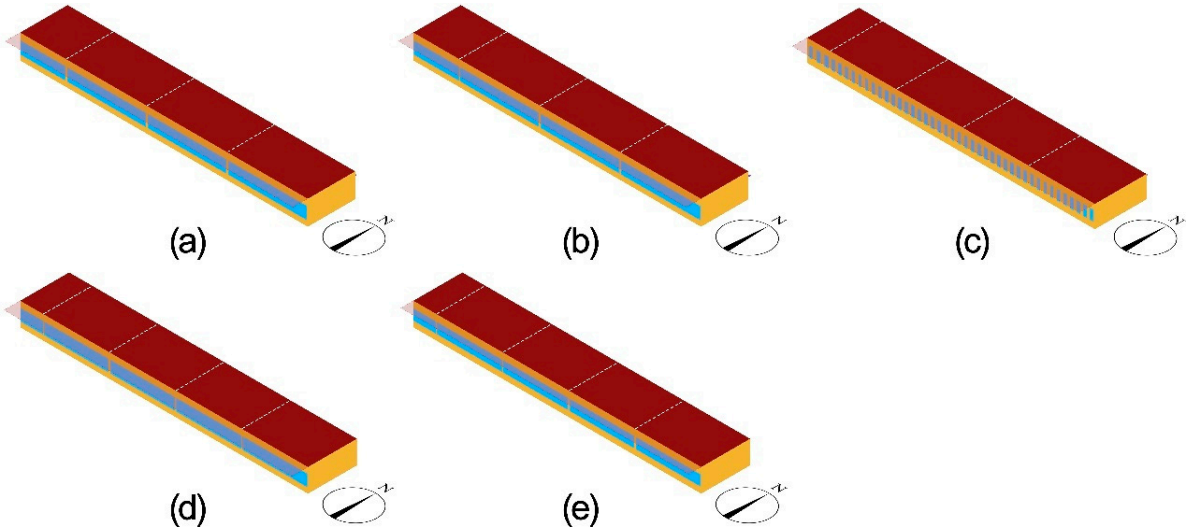

Figure 9. Parametric models of five design configurations for the south-facing corridor case: (**a**) sDA-Max solution, (**b**) UDI-Max solution, (**c**) Ec-Min solution, (**d**) overall optimal solution, and (**e**) baseline model.

The optimized solutions in Tables 7 and 8 were obtained by changing several design variables simultaneously. Their reductions in Ec relative to the baseline therefore reflect the combined adjustment of spatial dimensions, fenestration, glazing, shading, and other parameters; this study does not attribute those reductions to any single variable.

3.3. Classification Performance and Model Interpretation

Of the four classifiers, MLP performed best for both corridor orientations. Model selection and hyperparameter tuning were completed using the validation set, and the independent test set was used once after the model configuration had been fixed. As shown in Table 9, the test-set F1-scores were 0.979 for the south-facing corridor and 0.984 for the north-facing corridor. Five-fold cross-validation on the model-development data

provided an additional internal-stability check. For MLP, Precision, Recall, and F1-score were 0.941 ± 0.006, 0.944 ± 0.004, and 0.942 ± 0.002 for the south-facing corridor and 0.946 ± 0.004, 0.942 ± 0.004, and 0.944 ± 0.001 for the north-facing corridor. These cross-validation results describe internal validation within the current optimization dataset and are not treated as evidence of external generalizability.

Table 9. Test-set performance of four classification models under south- and north-facing orientations.

Classification Model	South-Facing Corridor Model (Test Set)			North-Facing Corridor Model (Test Set)		
	Precision	**Recall**	**F1-Score**	**Precision**	**Recall**	**F1-Score**
MLP	0.982	0.976	0.979	0.987	0.981	0.984
XGBoost	0.958	0.949	0.953	0.964	0.955	0.959
LightGBM	0.931	0.918	0.924	0.938	0.924	0.931
SVM	0.894	0.876	0.885	0.901	0.882	0.891

Considering the evaluation metrics and the loss curves shown in Figure 10, MLP had the strongest overall classification performance. SHAP analysis was then applied to all four classifiers to examine the consistency of feature-contribution rankings and directions across models.

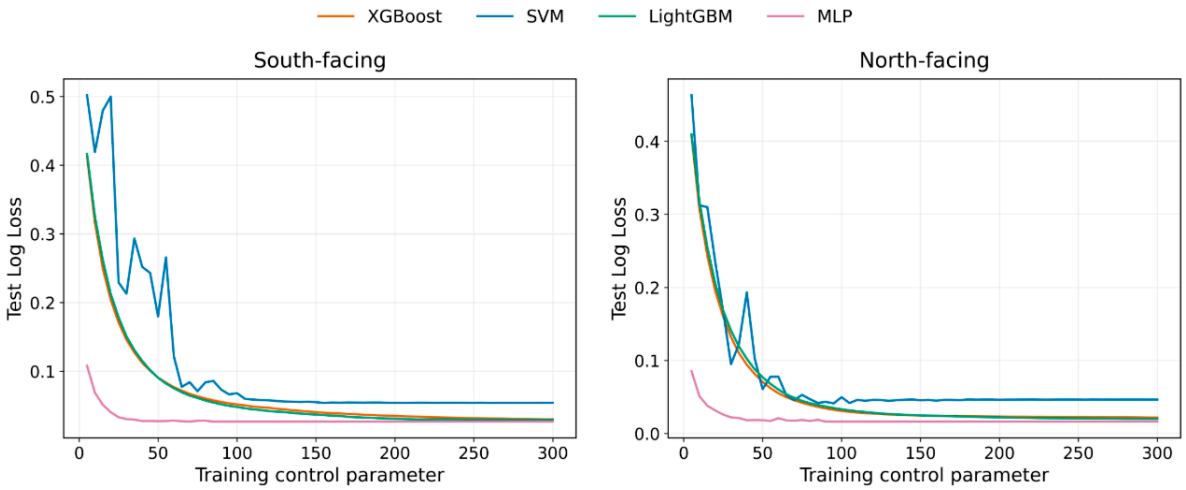

Figure 10. Training and validation diagnostics for the four classification models during model development.

For the model with a north-facing corridor (Figure 11), Classroom Depth (D_1) ranked first in all four models, including MLP, XGBoost, LightGBM, and SVM. D_1 affects the daylight penetration distance and spatial width, and therefore shows strong discriminative power within the coupled multi-objective optimization of daylighting and cooling performance. Corridor-side WWR (WWR_c) directly controls the daylight opening area on the side shaded by the exterior corridor and consequently maintains a relatively high contribution. WWR_c and Corridor Width (W_2) were also important design parameters affecting the daylighting and thermal performance of the north-facing corridor configuration, with contributions of 16.6–26.2% and 8.9–11.0%, respectively. The glazing-type parameters showed moderate contributions, whereas Exterior Window Height (H_2), Exterior Window Sill Height (H_3), and Exterior Window Pier Width (W_3) made relatively small contributions. As shown in Figure 11, low D_1, high WWR_c, and low W_2 values were mainly distributed in the positive SHAP region for the model with a north-facing corridor, indicating that these parameter settings were favorable for the coordinated improvement of daylighting and thermal performance. In contrast, high D_1, low WWR_c, and high W_2 values occurred more

frequently in the negative SHAP region. These results indicate that a shallower classroom depth (D_1), a higher corridor-side WWR (WWR_c), and a smaller corridor width (W_2) favor classification into the high-performance category.

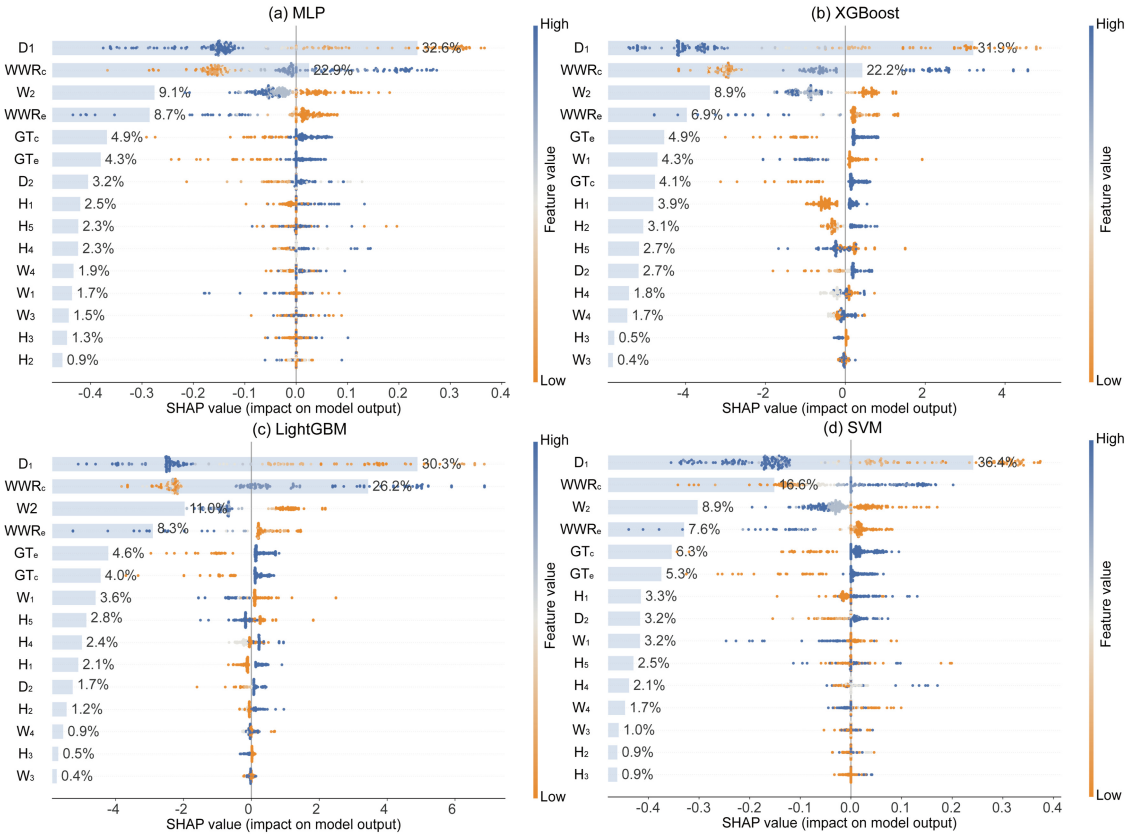

Figure 11. SHAP summary plots for the classification models of the north-facing corridor: (**a**) SHAP contributions of MLP; (**b**) SHAP contributions of XGBoost; (**c**) SHAP contributions of LightGBM; (**d**) SHAP contributions of SVM.

For the south-facing corridor, Figure 12 shows that feature importance is concentrated on the corridor-side facade. Corridor-side WWR (WWR_c) ranks first in all four models, with contributions ranging from 28.4% to 41.5%, while Corridor Window Pier Width (W_4) consistently ranks second, with contributions of 11.3% to 17.0%, followed by H_1, D_1, and W_2. With the shading effect provided by the south-facing corridor, the proportion of corridor-side windows and the window-pier configuration become the main information used by the models to identify high-performance solutions. In the SHAP interpretation, high WWR_c values consistently correspond to positive SHAP values, with the same direction observed across all four models. In contrast, high values of Corridor Window Pier Width (W_4) are mainly associated with negative SHAP values, indicating that a smaller W_4 is more favorable for predicting high-performance solutions. Higher Floor Height (H_1) and lower Classroom Depth (D_1) also contribute mainly positively. For Corridor Width (W_2), higher values tend to have positive SHAP contributions, opposite to the positive contribution associated with lower values in the north-facing model. This indicates that the favorable range of corridor width changes with corridor orientation. Overall, the north-facing model depends more on Classroom Depth (D_1) and the corridor-side WWR, whereas the south-facing model is more strongly associated with the joint configuration of Corridor-side WWR (WWR_c) and Corridor Window Pier Width (W_4).

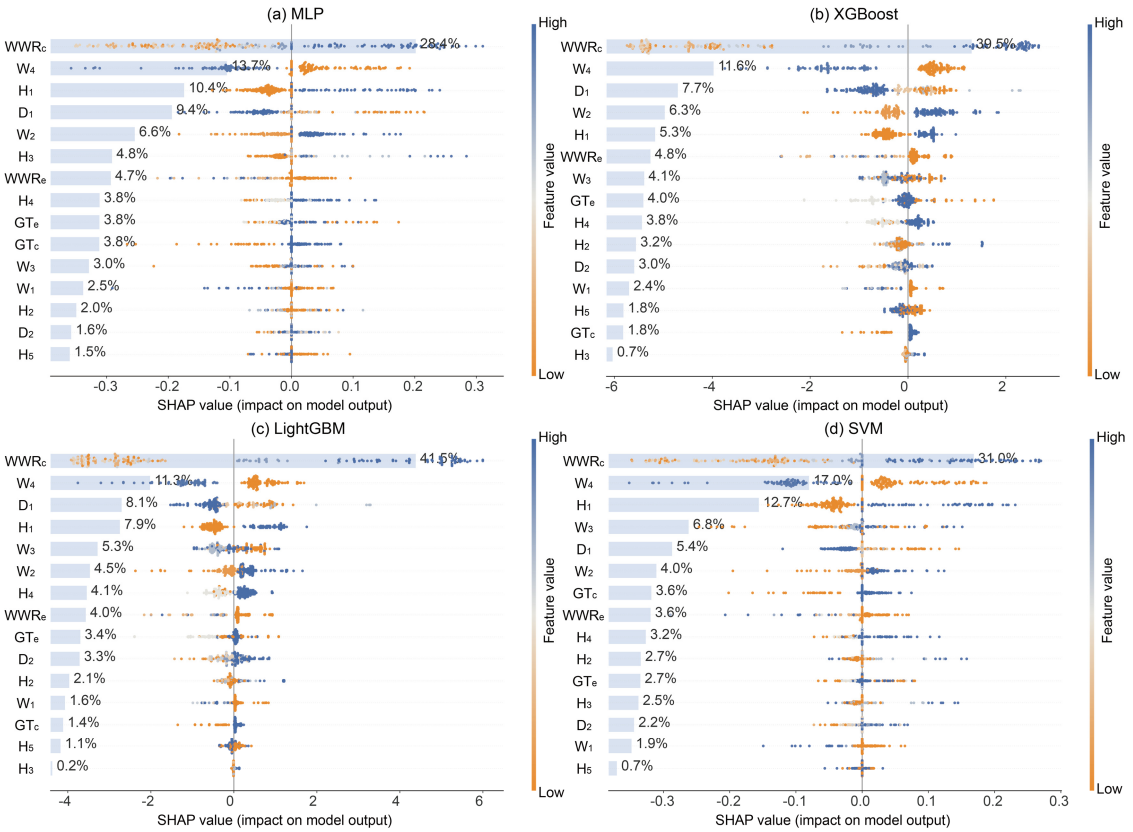

Figure 12. SHAP summary plots for the classification models of the south-facing corridor: (**a**) SHAP contributions of MLP; (**b**) SHAP contributions of XGBoost; (**c**) SHAP contributions of LightGBM; (**d**) SHAP contributions of SVM.

4. Discussion

4.1. Orientation-Dependent Differences in Favorable Parameter Distributions and Performance Improvements

Previous studies of educational buildings have used parametric simulation and multi-objective optimization to examine how classroom geometry, window-to-wall ratio, glazing type, shading dimensions, and orientation affect daylighting and energy performance [54,55]. These studies have identified favorable combinations of window, shading, and spatial parameters for different climates and building orientations; multi-objective optimization for educational-building performance design is therefore well established. The aim here is not to propose a new optimization algorithm. Rather, using the same linear teaching-building prototype and consistent simulation boundary conditions, we compare whether the favorable distributions of the same design variables remain stable when the exterior corridor is moved from the north to the south side.

The difference between the two corridor configurations was not simply that they produced separate sets of optimized designs. Within the Pareto solution sets, classroom depth (D_1), corridor width (W_2), corridor-side window-to-wall ratio (WWR_c), and Corridor Window Pier Width (W_4) showed different distributions. Thus, changing corridor orientation also changed favorable combinations of design variables, and parameter priorities derived for one configuration should not be applied directly to the other. Compared with the common baseline, the overall optimal north-facing-corridor solution increased sDA and UDI by 13.83% and 14.00%, respectively, and reduced Ec by 12.35%; the south-facing-corridor solution increased sDA and UDI by 9.04% and 2.60% and reduced Ec by 19.40%. These changes arose from joint optimization of several parameters. We therefore do not assign the reduction in Ec to the independent effect of any one spatial, glazing, or shading

variable. The first contribution is therefore the matched comparison of favorable parameter configurations and their associated performance gains under the two corridor orientations.

4.2. Differences in Parameter Contributions to High-Performance Classification Between Corridor Orientations

Recent building-performance studies have combined interpretable machine learning with multi-objective optimization to identify important design variables and their nonlinear responses [56,57]. SHAP itself is not presented as a methodological innovation here. Instead, it is used to compare whether the contribution rankings and directions of the same variables remain stable when spatial boundary conditions change. The SHAP results describe model attributions for prediction of the high-performance class, not strict causal relationships between individual variables and physical performance metrics.

The result of interest is not the expected change in solar exposure when corridor orientation changes, but whether the parameter priorities associated with high-performance solutions remain the same under common design variables and performance objectives. They did not: D_1 contributed most to high-performance classification in the north-facing-corridor model, followed by WWR_c; in the south-facing-corridor model, WWR_c was the leading variable, with W_4 and W_2 also becoming more prominent. The two prototypes therefore differed not only in parameter values but also in the combinations on which the classifiers relied to identify high-performance solutions. Within the design space studied, the result supports different parameter-adjustment priorities for the two corridor configurations. SHAP, however, reflects associations in model predictions, not causal effects of a single variable on sDA, UDI, or Ec. The contribution lies in this matched comparison of parameter-priority shifts, rather than in the SHAP method itself.

4.3. Rapid Daylighting and Cooling Performance Assessment for Early-Stage Design in Guangzhou

Machine-learning surrogates have been widely used to predict continuous building-performance outcomes, including energy use, indoor temperature, and illuminance [58,59], and classification has also been used for early-stage design assessment [60]. In this study, high-performance classes were defined separately from the multi-objective optimization results for the two corridor orientations. The third contribution is an orientation-specific classification model that converts these simulation and optimization results into rapid preliminary assessment information for university teaching buildings in Guangzhou.

Within the sampled design domain, the model allows a candidate parameter combination to be screened without repeating the full multi-objective optimization. SHAP identifies the variables that contribute most to high-performance classification in each orientation-specific model. The framework is an early-stage decision-support tool rather than a new machine-learning algorithm. Because the performance metrics were normalized separately and the high-performance labels were defined within each orientation dataset, the classifiers compare parameter contributions within orientations and do not establish an absolute performance ranking between them. They also do not replace Radiance or EnergyPlus in predicting individual performance metrics. Their labels derive from the combined assessment of physics-simulated sDA, UDI, and Ec, so the models provide only a rapid indication of parameter combinations with relatively high overall performance potential under the Guangzhou case conditions examined here.

4.4. Limitations and Future Work

Although the framework accounts for orientation differences in linear teaching buildings with exterior corridors, its scope has several limits. First, the optimization considers sDA, UDI, and Ec but does not directly include glare, natural ventilation, thermal comfort,

or stochastic occupant behavior. Second, the survey, measurements, and parametric models focus on the principal north- and south-facing classroom and corridor configurations observed in the Guangzhou sample. East- and west-facing cases were outside the current comparison. Because these façades receive low-angle solar radiation in the morning or afternoon, their solar gains, shading requirements, and daylight distribution may differ from those of the north- and south-facing cases. Future work will establish corresponding east- and west-facing prototypes and compare all four orientations in greater detail. Third, cooling was selected as the energy objective because the surveyed Guangzhou buildings operate in a hot-summer and warm-winter climate with limited heating demand. The reported parameter ranges should therefore not be transferred directly to heating-dominated regions. Finally, the quantitative findings apply to the sampled design domain and Guangzhou case conditions. The parametric modeling, multi-objective optimization, and classification workflow may be transferred to other educational-building contexts, but the numerical parameter ranges and performance improvements require cross-city and cross-climate validation. Future studies will survey teaching buildings in additional cities and climate zones, construct local parametric models, use location-specific EnergyPlus Weather (EPW) files, adapt heating and cooling objectives to local conditions, and test the classifiers with independently generated and simulated designs.

This study evaluates daylighting and cooling performance primarily through spatial daylight autonomy (sDA), useful daylight illuminance (UDI), and cooling energy consumption intensity (Ec). The useful UDI range is 100–2000 lx. Its upper bound captures some periods of excessive illuminance and can indicate potential visual discomfort to a degree, but cannot replace a dedicated glare metric. Likewise, Ec measures cooling energy use and does not directly represent indoor thermal comfort. To limit the number of objectives in the present optimization, separate glare and thermal-comfort metrics were not included. Future work will add these evaluations to examine overall indoor environmental performance under different corridor orientations.

The population size, generation count, crossover probability, and mutation probability were selected with reference to commonly used NSGA-II settings in related building-performance optimization studies and were applied consistently to both corridor orientations. The reviewer-suggested sensitivity analysis would nevertheless provide additional evidence on convergence and the stability of the reported parameter distributions. Because one complete optimization run required approximately five days, multi-seed tests were not feasible within the current computational budget. Future work will compare independent random seeds, population sizes, and generation counts and evaluate the consistency of Pareto fronts and key parameter distributions.

In addition, the stratified five-fold cross-validation in this study assessed the classifiers only within the existing optimization dataset. Although a held-out test set was used, its samples also came from the optimization history. These results therefore do not establish whether the favorable design-parameter ranges or the feature-importance rankings for north- and south-facing exterior-corridor configurations would remain stable across independent optimization runs or different samples. The findings remain limited to the sampled design domain and operating conditions of the Guangzhou case. Future work will compare parameter distributions and feature rankings from independent optimization runs with different random seeds and assess the classifiers using separately generated and simulated design cases.

5. Conclusions

Based on field measurements of typical classrooms in linear teaching buildings with exterior corridors in Guangzhou, this study combined parametric modeling, NSGA-II

multi-objective optimization, and machine-learning classification to compare the principal north- and south-facing corridor configurations. The conclusions are limited to the sampled design domain and the Guangzhou climate and operating conditions.

(1) In the south-facing-corridor model, classroom depth (D_1) was mainly 8.5–9.0 m and corridor width (W_2) was 2.6–2.8 m; in the north-facing-corridor model, D_1 ranged from 8.5 to 10.0 m and W_2 from 2.2 to 2.6 m. (2) Relative to the baseline, the overall optimal north-facing-corridor solution increased sDA and UDI by 13.83% and 14.00%, respectively, and reduced Ec by 12.35%; the south-facing-corridor solution increased sDA and UDI by 9.04% and 2.60% and reduced Ec by 19.40%. These improvements reflect the combined effect of optimizing multiple parameters, not an independent contribution from any one parameter. (3) The variables associated with prediction of the high-performance class ranked differently for the two corridor configurations. D_1 contributed most in the north-facing-corridor model, followed by WWR_c; WWR_c contributed most in the south-facing-corridor model, where W_4 and W_2 became relatively more important. Within the sampled design domain of this Guangzhou case, the two configurations therefore call for different design-parameter priorities. (4) The MLP achieved F1 scores of 0.979 and 0.984 and recall values of 0.976 and 0.981 on the two test sets. The combination of NSGA-II and MLP allows designers to rapidly screen design solutions with relatively high potential for synergistic daylighting and thermal performance at the early design stage, while translating orientation differences into design guidance for parameter adjustment.

Author Contributions: Conceptualization, S.M.; Methodology, S.M. and X.T.; Software, S.M. and M.Y.; Validation, S.M.; Formal Analysis, S.M.; Investigation, S.M. and M.Y.; Resources, S.M.; Data Curation, S.M. and M.Y.; Writing—Original Draft Preparation, S.M.; Writing—Review & Editing, S.M. and X.T.; Visualization, S.M. and M.Y.; Supervision, S.M.; All authors have read and agreed to the published version of the manuscript.

Funding: This research received no external funding.

Data Availability Statement: The data used in this study were acquired from our own experimental simulations.

Conflicts of Interest: The authors declare no conflicts of interest.

Nomenclature

Symbol	Meaning
D_1	Classroom Depth
W_1	Classroom Width
H_1	Floor Height
θ	Orientation
W_2	Corridor Width
H_2	Exterior Window Height
H_3	Exterior Window Sill Height
W_3	Exterior Window Pier Width
H_4	Corridor Window Height
H_5	Corridor Window Sill Height
W_4	Corridor Window Pier Width
WWR	Window-to-Wall Ratio
WWR_c	Corridor-side Window-to-Wall Ratio
WWR_e	Exterior Window-to-Wall Ratio
GT_e	Exterior Glazing Type
GT_c	Corridor-side Glazing Type
sDA	Spatial Daylight Autonomy

UDI	Useful Daylight Illuminance
Ec	Cooling Energy Consumption Intensity
SHGC	Solar Heat Gain Coefficient
COP	Coefficient of Performance
NSGA-II	Non-dominated Sorting Genetic Algorithm II
XGBoost	Extreme Gradient Boosting
LightGBM	Light Gradient Boosting Machine
SVM	Support Vector Machine
MLP	Multilayer Perceptron
SHAP	SHapley Additive exPlanations
R^2	Coefficient of Determination
MAPE	Mean Absolute Percentage Error
EPW	EnergyPlus Weather
D_2	Exterior Shading Depth

References

1. United Nations Environment Programme. *Global Alliance For Buildings And Construction Building Fast. Falling Short. As Climate Risks Rise and Cities Grow, We Must Rethink How We Build to Create Better Lives for All: Global Status Report for Buildings and Construction 2025-2026*; United Nations Environment Programme: Nairobi, Kenya, 2026.
2. Deng, J.-Y.; Xia, Y.; Lao, H.; Ye, Y.; Wang, Z.; Jiang, H. Natural Ventilation Potential of Teaching Building Complexes with Different Block Shapes and Layout Patterns. *J. Build. Eng.* **2024**, *96*, 110420. [CrossRef]
3. Yang, J.; Guo, T.; Wen, J.; Zhang, H.; Zhao, Y. The Impact of External Corridor Orientation and Shading Component Configuration on Thermal Comfort—A Case Study in the Hot–Humid Regions of China. *Environ. Dev. Sustain.* **2025**. [CrossRef]
4. Guo, W.; Liang, S.; He, Y.; Li, W.; Xiong, B.; Wen, H. Combining EnergyPlus and CFD to Predict and Optimize the Passive Ventilation Mode of Medium-Sized Gymnasium in Subtropical Regions. *Build. Environ.* **2022**, *207*, 108420. [CrossRef]
5. Ma, X.; Chen, H.; Lu, Y.; Luo, Q.; Yan, F.; Li, T.; Zhao, J.; Ding, H. Evaluating Blue-Green Infrastructure for Outdoor Thermal Comfort and Energy Efficiency in a University Campus Microclimate: A Case Study from Xi'an, China. *Energy Build.* **2026**, *350*, 116640. [CrossRef]
6. Tabadkani, A.; Roetzel, A.; Li, H.X.; Tsangrassoulis, A. Design Approaches and Typologies of Adaptive Facades: A Review. *Autom. Constr.* **2021**, *121*, 103450. [CrossRef]
7. Nazari, S.; Keshavarz Mirza Mohammadi, P.; Sareh, P. A Multi-objective Optimization Approach to Designing Window and Shading Systems Considering Building Energy Consumption and Occupant Comfort. *Eng. Rep.* **2023**, *5*, e12726. [CrossRef]
8. Khidmat, R.P.; Fukuda, H.; Paramita, B.; Koerniawan, M.D.; Kustiani, K. The Optimization of Louvers Shading Devices and Room Orientation under Three Different Sky Conditions. *J. Daylighting* **2022**, *9*, 137–149. [CrossRef]
9. Shi, Y.; Yang, Z.; Zheng, S.; Gao, D.; Yang, X. Multi-Objective Optimization of Embodied Carbon Emission, Energy Consumption, and Daylighting Performance of Educational Building in the Schematic Design Stage. *J. Build. Eng.* **2025**, *106*, 112594. [CrossRef]
10. Sedaghatnia, M.; Faizi, M.; Khakzand, M.; Sanaieian, H. Energy and Daylight Optimization of Shading Devices, Window Size, and Orientation for Educational Spaces in Tehran, Iran. *J. Archit. Eng.* **2021**, *27*, 04021011. [CrossRef]
11. Mangkuto, R.A.; Rohmah, M.; Asri, A.D. Design Optimisation for Window Size, Orientation, and Wall Reflectance with Regard to Various Daylight Metrics and Lighting Energy Demand: A Case Study of Buildings in the Tropics. *Appl. Energy* **2016**, *164*, 211–219. [CrossRef]
12. Ochoa, C.E.; Aries, M.B.C.; Van Loenen, E.J.; Hensen, J.L.M. Considerations on Design Optimization Criteria for Windows Providing Low Energy Consumption and High Visual Comfort. *Appl. Energy* **2012**, *95*, 238–245. [CrossRef]
13. Shen, H.; Tzempelikos, A. Daylighting and Energy Analysis of Private Offices with Automated Interior Roller Shades. *Sol. Energy* **2012**, *86*, 681–704. [CrossRef]
14. Zhai, Y.; Wang, Y.; Huang, Y.; Meng, X. A Multi-Objective Optimization Methodology for Window Design Considering Energy Consumption, Thermal Environment and Visual Performance. *Renew. Energy* **2019**, *134*, 1190–1199. [CrossRef]
15. Michael, A.; Heracleous, C. Assessment of Natural Lighting Performance and Visual Comfort of Educational Architecture in Southern Europe: The Case of Typical Educational School Premises in Cyprus. *Energy Build.* **2017**, *140*, 443–457. [CrossRef]
16. Zomorodian, Z.S.; Tahsildoost, M.; Hafezi, M. Thermal Comfort in Educational Buildings: A Review Article. *Renew. Sustain. Energy Rev.* **2016**, *59*, 895–906. [CrossRef]
17. Hwang, R.-L.; Lin, T.-P.; Kuo, N.-J. Field Experiments on Thermal Comfort in Campus Classrooms in Taiwan. *Energy Build.* **2006**, *38*, 53–62. [CrossRef]

18. Tzempelikos, A.; Athienitis, A.K. The Impact of Shading Design and Control on Building Cooling and Lighting Demand. *Sol. Energy* **2007**, *81*, 369–382. [CrossRef]
19. Pitts, A. Thermal Comfort in Transition Spaces. *Buildings* **2013**, *3*, 122–142. [CrossRef]
20. Zhang, A.; Bokel, R.; Van Den Dobbelsteen, A.; Sun, Y.; Huang, Q.; Zhang, Q. Optimization of Thermal and Daylight Performance of School Buildings Based on a Multi-Objective Genetic Algorithm in the Cold Climate of China. *Energy Build.* **2017**, *139*, 371–384. [CrossRef]
21. Al-Masrani, S.M.; Al-Obaidi, K.M.; Zalin, N.A.; Aida Isma, M.I. Design Optimisation of Solar Shading Systems for Tropical Office Buildings: Challenges and Future Trends. *Sol. Energy* **2018**, *170*, 849–872. [CrossRef]
22. Troup, L.; Phillips, R.; Eckelman, M.J.; Fannon, D. Effect of Window-to-Wall Ratio on Measured Energy Consumption in US Office Buildings. *Energy Build.* **2019**, *203*, 109434. [CrossRef]
23. Bakmohammadi, P.; Noorzai, E. Optimization of the Design of the Primary School Classrooms in Terms of Energy and Daylight Performance Considering Occupants' Thermal and Visual Comfort. *Energy Rep.* **2020**, *6*, 1590–1607. [CrossRef]
24. Talaei, M.; Sangin, H. Multi-Objective Optimization of Energy and Daylight Performance for School Envelopes in Desert, Semi-Arid, and Mediterranean Climates of Iran. *Build. Environ.* **2024**, *255*, 111424. [CrossRef]
25. Sun, Y.; Haghighat, F.; Fung, B.C.M. A Review of The-State-of-the-Art in Data-Driven Approaches for Building Energy Prediction. *Energy Build.* **2020**, *221*, 110022. [CrossRef]
26. Luo, J.; Zhuang, Z.; Bian, Y.; Wu, B.; Liang, G. Daylighting Performance Prediction Model for Linear Layouts of Teaching Building Clusters Utilizing Deep Learning. *Sustain. Cities Soc.* **2024**, *115*, 105821. [CrossRef]
27. Runge, J.; Zmeureanu, R. Forecasting Energy Use in Buildings Using Artificial Neural Networks: A Review. *Energies* **2019**, *12*, 3254. [CrossRef]
28. Tsanas, A.; Xifara, A. Accurate Quantitative Estimation of Energy Performance of Residential Buildings Using Statistical Machine Learning Tools. *Energy Build.* **2012**, *49*, 560–567. [CrossRef]
29. Amasyali, K.; El-Gohary, N.M. A Review of Data-Driven Building Energy Consumption Prediction Studies. *Renew. Sustain. Energy Rev.* **2018**, *81*, 1192–1205. [CrossRef]
30. Westermann, P.; Evins, R. Surrogate Modelling for Sustainable Building Design—A Review. *Energy Build.* **2019**, *198*, 170–186. [CrossRef]
31. Ahmad, M.W.; Mourshed, M.; Rezgui, Y. Trees vs Neurons: Comparison between Random Forest and ANN for High-Resolution Prediction of Building Energy Consumption. *Energy Build.* **2017**, *147*, 77–89. [CrossRef]
32. Singaravel, S.; Suykens, J.; Geyer, P. Deep-Learning Neural-Network Architectures and Methods: Using Component-Based Models in Building-Design Energy Prediction. *Adv. Eng. Inform.* **2018**, *38*, 81–90. [CrossRef]
33. Østergård, T.; Jensen, R.L.; Maagaard, S.E. A Comparison of Six Metamodeling Techniques Applied to Building Performance Simulations. *Appl. Energy* **2018**, *211*, 89–103. [CrossRef]
34. Geyer, P.; Singaravel, S. Component-Based Machine Learning for Performance Prediction in Building Design. *Appl. Energy* **2018**, *228*, 1439–1453. [CrossRef]
35. Fan, C.; Xiao, F.; Yan, C.; Liu, C.; Li, Z.; Wang, J. A Novel Methodology to Explain and Evaluate Data-Driven Building Energy Performance Models Based on Interpretable Machine Learning. *Appl. Energy* **2019**, *235*, 1551–1560. [CrossRef]
36. Zhou, C.; Wang, Z.; Wang, X.; Guo, R.; Zhang, Z.; Xiang, X.; Wu, Y. Deciphering the Nonlinear and Synergistic Role of Building Energy Variables in Shaping Carbon Emissions: A LightGBM- SHAP Framework in Office Buildings. *Build. Environ.* **2024**, *266*, 112035. [CrossRef]
37. Sadeghipour Roudsari, M.; Pak, M.; Viola, A. Ladybug: A Parametric Environmental Plugin for Grasshopper to Help Designers Create an Environmentally-Conscious Design. In Proceedings of the 13th Conference of International Building Performance Simulation Association, Chambery, France, 26–28 August 2013; pp. 3128–3135.
38. Ladybug Tools Honeybee. Available online: https://www.ladybug.tools/honeybee.html (accessed on 7 October 2026).
39. Ward, G.J. The RADIANCE Lighting Simulation and Rendering System. In Proceedings of the 21st Annual Conference on Computer Graphics and Interactive Techniques, Orlando, FL, USA, 24–29 July 1994; pp. 459–472.
40. Crawley, D.B.; Lawrie, L.K.; Winkelmann, F.C.; Buhl, W.F.; Huang, Y.J.; Pedersen, C.O.; Strand, R.K.; Liesen, R.J.; Fisher, D.E.; Witte, M.J.; et al. EnergyPlus: Creating a New-Generation Building Energy Simulation Program. *Energy Build.* **2001**, *33*, 319–331. [CrossRef]
41. Wallacei Evolutionary Engine for Grasshopper3D | Wallacei. Available online: https://www.wallacei.com/home (accessed on 7 October 2026).
42. *GB 50189-2015*; Design Standard for Energy Efficiency of Public Buildings. China Architecture & Building Press: Beijing, China, 2015.
43. Bian, Y.; Chen, Y.; Sun, Y.; Ma, Y.; Yu, D.; Leng, T. Simulation of Daylight Availability, Visual Comfort and View Clarity for a Novel Window System with Switchable Blinds in Classrooms. *Build. Environ.* **2023**, *235*, 110243. [CrossRef]

44. Chi, D.A.; Moreno, D.; Navarro, J. Correlating Daylight Availability Metric with Lighting, Heating and Cooling Energy Consumptions. *Build. Environ.* **2018**, *132*, 170–180. [CrossRef]
45. Nabil, A.; Mardaljevic, J. Useful Daylight Illuminances: A Replacement for Daylight Factors. *Energy Build.* **2006**, *38*, 905–913. [CrossRef]
46. Chen, T.; Guestrin, C. XGBoost: A Scalable Tree Boosting System. In *Proceedings of the 22nd ACM SIGKDD International Conference on Knowledge Discovery and Data Mining, San Francisco, CA, USA, 13–17 August 2016*; Association for Computing Machinery: New York, NY, USA, 2016; pp. 785–794.
47. Ke, G.; Meng, Q.; Finley, T.; Wang, T.; Chen, W.; Ma, W.; Ye, Q.; Liu, T.-Y. LightGBM: A Highly Efficient Gradient Boosting Decision Tree. In *Proceedings of the Advances in Neural Information Processing Systems 30, Long Beach, CA, USA, 4–9 December 2017*; Curran Associates, Inc.: Red Hook, NY, USA, 2017; Volume 30, pp. 3146–3154.
48. Yang, B.; Li, X.; Liu, Y.; Chen, L.; Guo, R.; Wang, F.; Yan, K. Comparison of Models for Predicting Winter Individual Thermal Comfort Based on Machine Learning Algorithms. *Build. Environ.* **2022**, *215*, 108970. [CrossRef]
49. Langtry, M.; Wichitwechkarn, V.; Ward, R.; Zhuang, C.; Kreitmair, M.J.; Makasis, N.; Xuereb Conti, Z.; Choudhary, R. Impact of Data for Forecasting on Performance of Model Predictive Control in Buildings with Smart Energy Storage. *Energy Build.* **2024**, *320*, 114605. [CrossRef]
50. Barandier, P.; Mendes, M.; Marques Cardoso, A.J. Comparative Analysis of Four Classification Algorithms for Fault Detection of Heat Pumps. *Energy Build.* **2024**, *316*, 114342. [CrossRef]
51. Both, M.; Kämper, B.; Cartus, A.; Beermann, J.; Fessler, T.; Müller, J.; Diedrich, C. Automated Monitoring Applications for Existing Buildings through Natural Language Processing Based Semantic Mapping of Operational Data and Creation of Digital Twins. *Energy Build.* **2023**, *300*, 113635. [CrossRef]
52. Mayer, K.; Haas, L.; Huang, T.; Bernabé-Moreno, J.; Rajagopal, R.; Fischer, M. Estimating Building Energy Efficiency from Street View Imagery, Aerial Imagery, and Land Surface Temperature Data. *Appl. Energy* **2023**, *333*, 120542. [CrossRef]
53. Shams Amiri, S.; Mueller, M.; Hoque, S. Investigating the Application of a Commercial and Residential Energy Consumption Prediction Model for Urban Planning Scenarios with Machine Learning and Shapley Additive Explanation Methods. *Energy Build.* **2023**, *287*, 112965. [CrossRef]
54. Lakhdari, K.; Sriti, L.; Painter, B. Parametric Optimization of Daylight, Thermal and Energy Performance of Middle School Classrooms, Case of Hot and Dry Regions. *Build. Environ.* **2021**, *204*, 108173. [CrossRef]
55. Xue, P.; Li, Q.; Xie, J.; Zhao, M.; Liu, J. Optimization of Window-to-Wall Ratio with Sunshades in China Low Latitude Region Considering Daylighting and Energy Saving Requirements. *Appl. Energy* **2019**, *233–234*, 62–70. [CrossRef]
56. Wang, Y.; Xing, R.; Yang, Y.; Ren, J.; Zhou, M.; Zhao, J.; Cheng, X.; Ma, X. Morphology–Crowd Coupling and Mitigation of Pedestrian-Level PM2.5 Exposure in Summer Night Markets: Interpretable Machine Learning and CFD across Compact LCZs. *Build. Environ.* **2026**, *304*, 115107. [CrossRef]
57. Shen, Y.; Pan, Y. BIM-Supported Automatic Energy Performance Analysis for Green Building Design Using Explainable Machine Learning and Multi-Objective Optimization. *Appl. Energy* **2023**, *333*, 120575. [CrossRef]
58. Westermann, P.; Welzel, M.; Evins, R. Using a Deep Temporal Convolutional Network as a Building Energy Surrogate Model That Spans Multiple Climate Zones. *Appl. Energy* **2020**, *278*, 115563. [CrossRef]
59. Ali, A.; Jayaraman, R.; Mayyas, A.; Alaifan, B.; Azar, E. Machine Learning as a Surrogate to Building Performance Simulation: Predicting Energy Consumption under Different Operational Settings. *Energy Build.* **2023**, *286*, 112940. [CrossRef]
60. Yan, H.; Yan, K.; Ji, G. Optimization and Prediction in the Early Design Stage of Office Buildings Using Genetic and XGBoost Algorithms. *Build. Environ.* **2022**, *218*, 109081. [CrossRef]

Disclaimer/Publisher's Note: The statements, opinions and data contained in all publications are solely those of the individual author(s) and contributor(s) and not of MDPI and/or the editor(s). MDPI and/or the editor(s) disclaim responsibility for any injury to people or property resulting from any ideas, methods, instructions or products referred to in the content.